

Université de Montréal

**The potential role of the multivalent ionic compound PolyP in the
assembly of the liquid nature in the cell**

par

Lara Michel Matta

Département de Biochimie et Médecine Moléculaire

Faculté de Médecine

Mémoire présenté à la Faculté de Médecine

en vue de l'obtention du grade de Maître ès Sciences (M.Sc.)

En Biochimie

Option cheminement libre

November 2016

© Lara Michel Matta, 2016

Résumé

Les protéines de type prion, contenant des Séquences en acides aminés de Faible Complexité (SFC), ont tendance à s'agréger et à former des compartiments non-membranaires dans la cellule. Ces derniers ont des propriétés physiques communes à celles des liquides, telles que la capacité de mouiller les surfaces, de s'écouler et de fusionner avec d'autres corps liquides. Dans cette étude, nous avons démontré que la protéine Hrp1 forme, *in vitro*, des gouttes de différentes tailles *via* une transition de phase liquide à liquide, et ce, uniquement lorsqu'elle est exposée à un milieu chargé négativement. Exclusivement dans ce même milieu, nous avons aussi observé que le domaine SFC de Hrp1 s'assemble et forme une matière de type gel. Sur la base de ces observations, nous avons émis l'hypothèse que la tendance des systèmes moléculaires à former des compartiments liquides *in vivo* peut être influencée par la présence, dans le cytosol, de polyélectrolytes chargés négativement tels que l'ADN, l'ARN et les polyphosphates (PolyP). En utilisant la levure comme modèle cellulaire et des techniques de microscopie à fluorescence, nous nous sommes focalisés sur l'étude du rôle des PolyP dans l'assemblage des P-bodies. Les P-bodies ont été choisis comme système moléculaire de référence *in vivo*, étant des corps qui, après une transition de phase, se trouvent dans le cytosol sous forme de gouttes. Nous avons démontré que la déplétion du phosphate et la délétion du gène *vtc4*, responsable de la synthèse des PolyP dans la levure, n'ont pas d'influence dans la formation des P-bodies. Nous avons aussi remarqué que les PolyP et la protéine Edc3, une des composantes principales des P-bodies, ne sont pas co-localisés dans la cellule. Cette étude préliminaire nous suggère un manque de corrélation entre la formation des P-bodies et la présence de PolyP dans la cellule. Cependant, pour confirmer nos observations, des expériences complémentaires doivent être envisagées, en considérant d'autres composantes des P-bodies, tel que Lsm4, ou en analysant, *in vivo*, les effets des PolyP sur d'autres systèmes moléculaires de nature liquide.

Mots-clés : les protéines de type prion, séquence de faible complexité, les gouttes liquides, matière de type gel, PolyP, transition de phase liquide à liquide.

Abstract

Prion-like proteins containing Low Complexity Sequences (LCSs) have the propensity to aggregate and form membrane-less compartments in the cell. These proteins form droplets that have liquid features such as wetting, dripping and fusion. In this study, we demonstrated that the prion domain-containing protein Hrp1 forms droplets of different sizes in the presence of negatively charged polymers *via* liquid-liquid phase separation, whereas under the same conditions, the prion-like domain PolyQ/N of Hrp1 forms a gel-like material. Based on these findings, we hypothesize that droplets *in vivo* could be modulated by negatively charged polyelectrolytes found in the cell such as DNA, RNA and polyphosphate (PolyP). My goal was to examine the role of the polyanionic nature of PolyP on the assembly of P-bodies using *Saccharomyces cerevisiae* as a cellular model and fluorescence microscopy. We chose to study processing (P)- bodies, based on previous findings that these cellular subcompartments are formed by liquid-liquid phase separation of component proteins in the cytoplasm. We found that depleting phosphate from the media and deleting *vtc4* gene, which is responsible for PolyP synthesis, did not have any effect on P-body formation. In addition, we demonstrated that PolyP and the protein Edc3, a core component of P-bodies, do not co-localize. Our data suggest that PolyP does not affect P-body formation. However, further and complementary studies have to be performed to confirm that PolyP have no effects on other membrane-less organelles.

Keywords: Prion like proteins, Low Complexity Sequence, droplet, gel-like material, PolyP, liquid-liquid phase separation.

List of Contents

Résumé.....	i
Abstract.....	ii
List of Contents.....	iii
List of Tables	v
List of Figures.....	vi
Abbreviation	vii
Acknowledgment	ix
1 Introduction.....	1
1.1 Proteins containing low complexity sequence domains can undergo liquid-liquid phase separation to form membrane-less organelles.....	2
1.2 The Prion like protein Hrp1 forms visible aggregates.....	12
1.3 The P-body is a liquid droplet.....	13
1.4 The role of the multivalent ionic compound polyphosphate in the cell.....	16
1.5 Research project.....	19
1.5.1 Problematic and hypothesis	19
1.5.2 Objectives	21
1.5.3 The techniques used in this study	21
2 Materials and Methods.....	21
2.1 Media	22
2.2 Strains and Plasmids	22
2.3 The designed primers for different experiments.....	23
2.4 Extraction of yeast genomic DNA.....	24
2.5 Overexpression and purification of Hrp1 and its variants	25
2.6 Circular Dichroism Spectroscopy	26
2.7 Transmission Electron Microscope analysis.....	26
2.8 Design a cassette for homologous recombination to replace the gene to be deleted with an antibiotic as a selection marker	26
2.9 Homologous Recombination	27

2.10	Observation of P-bodies in mid-log glucose starved cells.....	28
2.11	Detection of PolyP with DAPI staining using the fluorometer.....	28
2.12	P-body analysis and quantification of number and size.....	29
2.13	Statistical analysis.....	30
3	Results.....	31
3.1	Polyanionic molecules induce liquid-liquid phase separation of the RNA binding Protein Hrp1 <i>in vitro</i>	32
3.2	Hrp1 is largely in an alpha helical conformation.....	36
3.3	Phosphate depletion has no effect on P-body formation	38
3.4	Deletion of <i>vtc4</i> increases P-body numbers.....	42
3.5	The PolyP does not associate with the P-body core component Edc3	46
4	Discussion.....	48
5	Conclusion and Perspectives.....	54
6	References.....	56
7	Appendix.....	63
7.1	Supplementary figures	64
7.2	Dhh1 protein forms droplets under physiological salt concentration	68

List of Tables

Table 2.1. Bacterial and yeast strains	22
Table 2.2. Plasmids for protein expressions and gene deletion	23
Table 2.3. PCR primers for <i>in vitro</i> and <i>in vivo</i> studies	23

List of Figures

Figure 1.1. The features of prion like proteins	4
Figure 1.2. The morphological and physical differences between gel-like and liquid-like materials .	8
Figure 1.3 Different types of interactions that trigger liquid-liquid phase separation	10
Figure 1.4 Model for P-body assembly.....	15
Figure 1.5 Pathway of Inositol pyrophosphate and polyphosphate metabolism.....	18
Figure 3.1. Hrp1 purification approach.....	33
Figure 3.2. Induction of Hrp1 droplets is a concentration-dependent and sensitive to polyanionic molecules.....	35
Figure 3.3. Hrp1 is predominantly helical.....	37
Figure 3.4. Phosphate depletion has no effect on P-body number and size.....	41
Figure 3.5. Deletion of <i>vtc4</i> gene leads to an increase in the number of P-bodies per cell	45
Figure 3.6. PolyP does not associate with P-bodies.....	47
Fig.S 7.1 Scheme for Hrp1 purification and its variants	65
Fig.S 7.2.SDS-PAGE of RRM and PrD after affinity chromatography and Size exclusion chromatography.....	66
Fig.S 7.3. Screening for droplet formation.....	67
Fig.S 7.4. Dhh1 protein forms droplets under NaCl physiological conditions.....	68

Abbreviation

BSA	Bovine Serum Albumine
BNI1	Formin encoding mRNA
CD	Circular Dichroism
FG	Phenylalanine Glycine repeats
FRAP	Fluorescence After Photobleaching
FUS	Fusion in Sacroma protein
G	Glycine
HMM	Hidden Markov Model algorithm
HLM	Helical Leucine Motif
hnRNPA1	Heterogeneous nuclear Ribonucleoprotein A1
IP (1-7)	Inositol pyrophosphate (1-7)
K	Lysine
LCS/D	Low complexity Sequence/Domain
LLPS	Liquid-Liquid phase separation
MEG1/3	Maternal-Effect Germline 1/3
MW	Molecular weight
NPC	Nuclear pore complex
Nsr1	Nuclear Signal Recognition 1
OD	Optical Density
P	Proline
PKK1	polyphosphate kinases 1
PolyP	polyphosphate
PolyQ/N	Poly (Glutamine/Asparagine)
Ppx1, Ppn1	Exopolyphosphatases
PrD	Prion forming Domain
PRM	Proline Rich motif
PTB	Polypyrimidine Tract Binding Protein

RGG	Arginine Glycine Box
RNA	Ribose Nucleic Acid
RRM	RNA Recognition Motif
RT	Room Temperature
S	Serine
SD	Synthetic Dextrose Media
SDS	Sodium Dodecyl Sulfate
SEC	Size exclusion chromatography
SGD	<i>Sacharomyces</i> Genome Database
SH3	SRC homology 3
thT	Thioflavin dye
TEM	Transmission Electron Microscopy
TOP1	Topoisomerase 1
5' UTR	5' Untranslated Region
3' UTR	3' Untranslated Region
<i>Vtc</i> (1-4)	Vacuolar Transporter Chaperone (1-4)
Y	Tyrosine

Acknowledgment

First, I would like to thank my supervisor Prof. Stephen W. Michnick, for giving me the chance to pursue my science training at the UdeM in his laboratory, despite the difficult start. Moreover, I thank him for being very patient with me and for giving me the time to reflect on, dream about, and spread my ideas. I would like also to thank my PhD committee Dr. Marlene Oeffinger and Dr. Alexis Vallée-Bélisle for their helpful comments during my last committee meeting. I am also grateful to my current thesis committee members, Professor Marlene Oeffinger and Professor Pascal Chartrand

In addition, I would like to express my gratitude to Dr. Cornelia Zorca, for her guidance throughout my academic years at UdeM, for all the scientific discussions that we had, and for encouraging me to ask focused questions with defined objectives.

I would like to thank my colleague in Prof. Michnick Laboratory, Dr. Durga Sivanesan, for the scientific discussions that we had during the long working hour in the laboratory, and for looking over my master thesis. I will always remember the fun Sushi nights. I would like also to thank Diala Abd Rabbo for spiritual and personal life coaching. I thank also Bram, Sinan, Luz, Emmanuelle, and our invited researcher Dr. Alessandra Nurisso for the funny talks and the good time that we spent at McCarold's. I also thank the angel and the engine of our laboratory Jacqueline Moreno Kovarzyk for calming me down when I began to jump in the laboratory with excitement.

Not to forget the engine of the department and the lovely lady, Madame Sylvie Beauchemin for making my life easier throughout my journey on campus.

Finally, I would like to thank the chemistry folk for letting me borrow materials without hesitation to perform my experiments, especially Jean Richard Bullet and Adeline Lafon from Prof. Françoise Winnick's laboratory and Julien from Prof. William D. Lubell's laboratory.

1 Introduction

1.1 Proteins containing low complexity sequence domains can undergo liquid-liquid phase separation to form membrane-less organelles

The cytoplasm of a eukaryotic cell is a complex crowded fluid where biochemical reactions and biochemical events take place in organelles that are maintained by membrane bound as well as membrane-less compartments. The assembly and the transport of molecules into and out of membrane delimited organelles, such as Golgi apparatus and the mitochondria, have been deciphered¹. In contrast, the chemical, and physical properties, and the organization of the heterogeneous matter that contributes to the assembly of the membrane-less organelles are still enigmatic^{1,2}. Both the nucleus and the cytoplasm contain membrane-less organelles. For instance, P-bodies and stress granules are found in the cytoplasm, while the nucleus contains the nucleolus, Cajal bodies and nuclear speckles.

Recently, the composition and specificity of the macromolecules within membrane-less organelles such as RNA-granules have been identified. RNA granules are involved in mRNA metabolism such as storage, splicing and modification. They consist mainly of an ensemble of mRNAs and RNA binding proteins. Interestingly, RNA binding proteins within these granules have RNA Recognition Motifs (RRMs) and Low Complexity sequences (LCSs)^{1,3,4}, meaning repetitive sequences composed of few amino acids, which could be the same amino acids or small stretches of few amino acids. These stretches are intrinsically disordered; i.e. they do not form well-defined structures. The composition of one class of LCSs is identical to that of the prion-forming domains (PrD) or the so-called prion like domain such as Poly Q/N (Glutamine/Asparagine). These domains consist of about 60 amino acids and are rich in uncharged polar residues such as Asparagine (Q), Glutamine (N), Serine (S), Proline (P), Glycine (G) and tyrosine (Y)^{1,5-9}. Despite the fact that these stretches are intrinsically disordered, they have the propensity to spontaneously self-assemble and to form highly ordered structures, amyloid fibrils. These are rich in β -sheets secondary structure and are connected through an internal network of stable hydrogen bonds. The self-templating amyloids contribute to phenotypic changes and this could be infectious, transmissible from one organism to another, which gives the feature of a prion^{1,10}. The prions can be harmful,

when they cause neurodegenerative diseases such as Parkinson's, or beneficial as yeast prions that might serve for diversifying the microbial population via a mechanism called bet hedging⁴.

Alberti *et al.* (2009) performed a proteomic screening in *Saccharomyces cerevisiae*, searching for prion candidates by using a Hidden Markov Model (HMM) algorithm¹¹. As a training model, Sup35 and Ure2 yeast prions were used. The former is a translation termination factor, while the latter is involved in Nitrogen metabolism. Both of these prions are enriched in PolyQ and PolyN stretches, respectively. These protein candidates were able to bind to thioflavin T dye (thT dye) over time, a property or feature known for the amyloid proteins. However, unlike amyloids, they depolymerize at very low detergent concentration (2% SDS)¹¹, implying that these protein assemblies are dynamic (**Figure 1.1**). They can switch from a soluble phase, the protein solution, which has the viscosity of water, to a more rigid state, the amyloid-like structure. Moreover, the implication of PolyQ/N in the formation of RNA granules has been elucidated. RNA binding proteins within these assemblies form fibrillar structure with amyloid like properties. PolyQ/N domains are intrinsically disordered and aggregation-prone^{12,13}. Lindquist *et al.* (2011) revealed via mutational experiments that the replacement of Q's with N's stimulates the formation of benign self-templating amyloids, whereas the substitution of N's with Q's triggers the formation of toxic, non-amyloid aggregates¹⁴. PolyQ stretches in Htt-exon1 (Huntington disease) protein causes neurodegenerative disorders above a threshold of 35 Qs. In contrast, ataxin-3 at a PolyQ length well above 50 Qs remains soluble and non-pathogenic¹³. The question that emerges is how the arrangement of the linear information (the primary sequence) could influence the behaviour and the nature of the protein. What is the stimulus, the switch or the fundamental principles that lead to such differences?

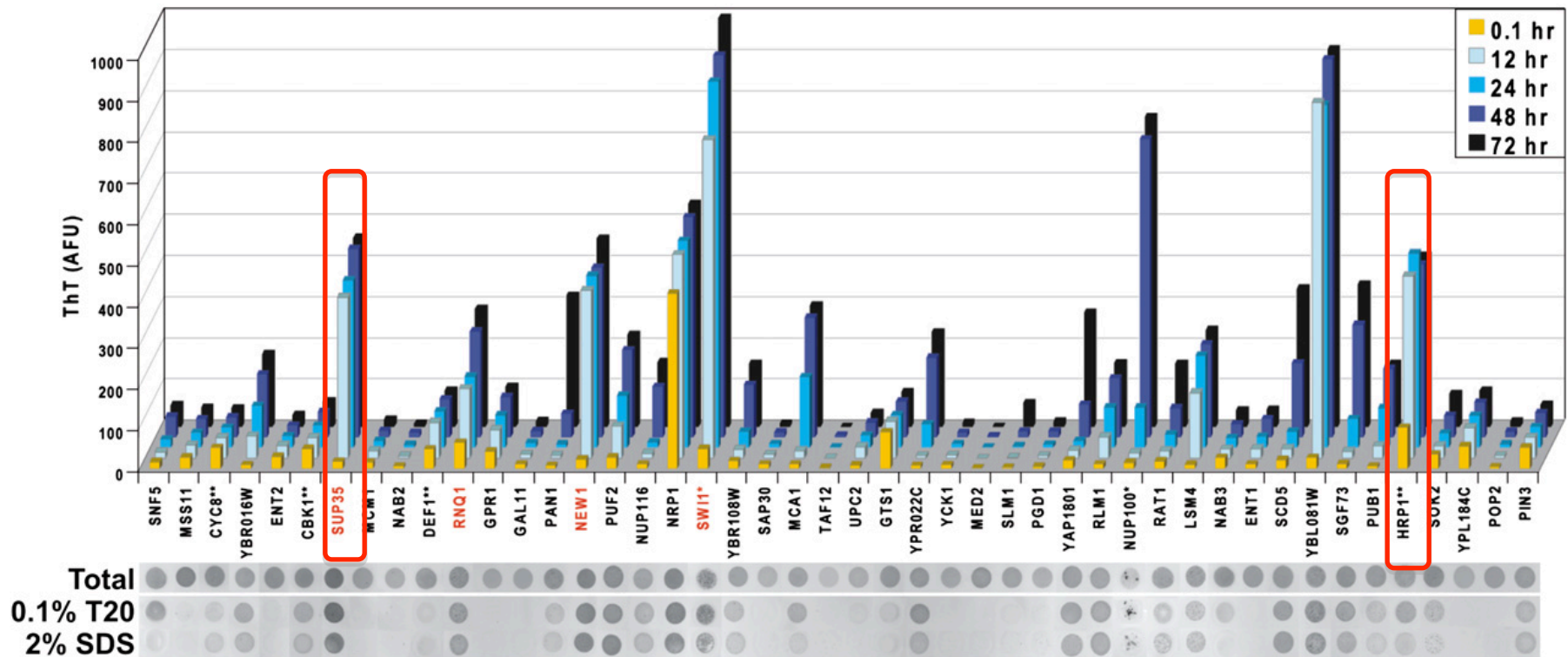


Figure 1.1. The features of prion like proteins

The prion protein sup35 binds to ThT dye over time and do not dissolve upon treatment with low concentration of detergent. Whereas, the prion like protein Hrp1, similarly to sup 35 binds to ThT dye, but dissolve under low concentration of detergent SDS (adapted from 11)

LCSs have been shown to undergo phase separation, where a liquid state, droplets, or gel-like material, hydrogel, formed (**Figure 1.2.a**). Hydrogels contain mainly water that tends to swell the gel and removing the water from the inside requires external forces. However, it has not yet been deciphered what are the arrangements and rearrangements of the primary sequences that trigger either the gel-like or the droplet states. Besides, it is still enigmatic why the cell chooses the liquid matter or the gel-like matter to convey information, signals or to organize heterogeneous matter in different organelles with different physical properties.

Han *et al.* (2012) revealed that the polymerization of LCSs triggers the formation of RNA granules, which consist of prion-like proteins, and consequently serve to localize mRNAs and in return can control spatial and temporal nature of translation. However, the structural transitions that prion-like proteins undergo and the regulation of these transitions are unknown^{3,4}. Han and co-workers revealed that the LCSs of the prion-like proteins undergo phase transitions, resulting in the formation of hydrogels. Their observation was confirmed using the N-terminal of FUS protein (fusion in sarcoma) as a model. The N-terminal domain of the RNA binding protein FUS consists of 27 repeats of the amino acid sequence Gly.Tyr.Ser. At high protein concentrations (~ 50 mg /ml), following incubation for one week at 4 °C, a FUS hydrogel was formed. Hydrogel formation takes place *via* homotypic or heterotypic interactions of the prion-like proteins, meaning, promiscuous interactions between prion-like proteins that have the same or distinct identities (**Figure 1.2.b**). The X-ray diffraction pattern of hydrogels shows a characteristic cross- β structure, where X-ray reflections were observed at 4.6 Å° and 10 Å°, and transmission electron microscopy (TEM) shows a well-defined filament (**Figure 1.2.c**). Similarly, the multivalent cohesive FG repeats (Phenylalanine-Glycine repeats) of the nuclear pore complex (NPC) was found to form a gel-like material at high concentrations namely 200 mg/ml with incubation for 24 hours at room temperature (RT). More importantly, this study found that the NQ sequence of the FG repeats triggers protein-protein interactions and that the FG-hydrogel is stabilized by β -structures^{15,16}. However, the question remains, does the intrinsically disordered region, namely the LCS PolyQ/N, form a hydrogel β -structure in the cytoplasm? Do macromolecular complexes of LCSs-containing proteins form gels in the cell?

In contrast to limited evidence of RNA binding proteins forming gels *in vitro* liquid droplets composed of these proteins have been demonstrated to form *via* liquid-liquid phase separation (**Figure 1.2.d**). The droplet is recognizable as separate and soluble aggregates of materials having different physical properties from those of the surrounding bulk; the cytosol. The phase separation enables the component of a biological system to rapidly concentrate in one place and the entry of other proteins or regulator could trigger the disassembly.

An interesting example of a droplet is the germ cell P-granules of *Caenorhabditis elegans* (*C. elegans*), which localize to the posterior of one cell-embryos and display liquid-like properties including wetting, dripping and fusion. The condensation and the dissolution of these assemblies, called P-granules, are triggered by a Mex5 protein gradient in the cytoplasm. Increasing the concentration of Mex5 within P-granule droplets led to dissolution of the droplets. FRAP analysis (Fluorescence Recovery After Photobleaching) revealed that the components forming these droplets are very dynamic, where exchange of material takes place between the bulk and the droplets on timescales of seconds to minutes¹⁷⁻¹⁹. Another interesting example is the storage of mTORC protein within stress granules, which inhibits its kinase. The activation of the DYRK3 kinase disassembles the stress granule and releases mTORC for signalling²⁰.

The collective behaviour of the prion-like proteins forming droplets is still enigmatic. A recent study demonstrated that multivalency is essential for droplet formation²¹. Multiple weak interactions, namely protein-protein and protein-mRNA interactions, lead to phase separation and droplets formation. This study used multimodular domains such as the SRC homology 3 (SH3) and Proline Rich Motif (PRM), where a tandem repeat of SH3_m and PRM_n (m,n :1-5) were separately engineered. The high affinity of SH3₁-PRM₁ monovalency blocks the phase transition, but by increasing the valency SH3₄-PRM₄ after few hours at high protein concentrations, phase separation occurred and droplets formed (**Figure 1.2.c**). Moreover, droplets were seen after two days by mixing the Polypyrimidine Tract Binding Protein (PTB) with RNA oligonucleotides. More importantly, the droplet was observed *in vitro* and *in vivo* as well and the cryo-electron microscopy analyses of the droplets display a well-defined ring shape (**Figure 1.2.e**)²¹. These observations suggest that the affinity of the interacting proteins and the valency are the tipping points for phase separation. The morphology, the structure and

physical properties of the liquid state formed *via* multiple weak interactions are completely different from that of the hydrogel.

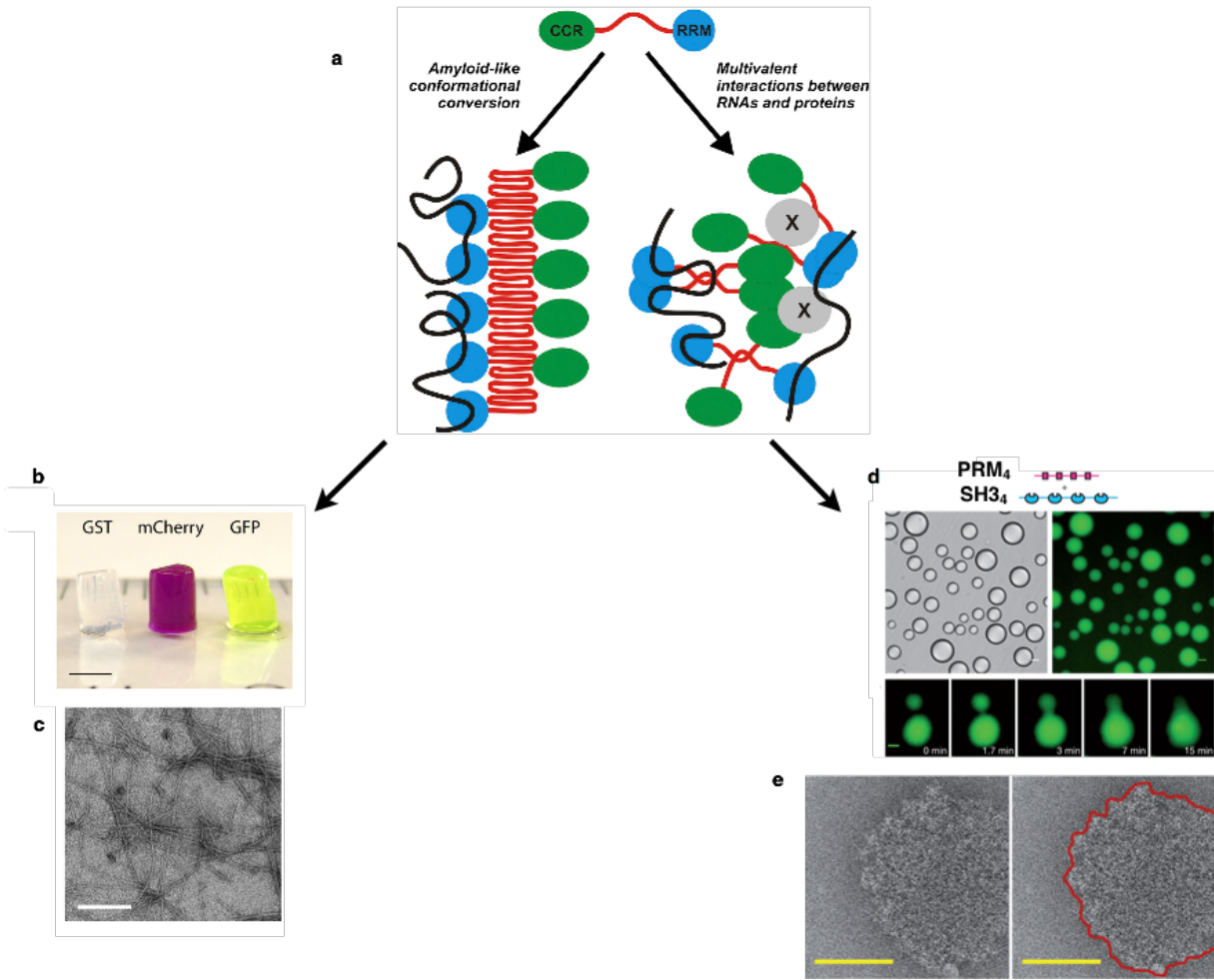


Figure 1.2. The morphological and physical differences between gel-like and liquid-like materials

a) Prion-like proteins containing LCSs and RRM tend to polymerize and form amyloid like structure or to undergo multiple weak interactions and undergo phase separation to form droplets. b) The LC domain of FUS protein labeled with different fluorophore, incubated for one week at 4 °C. c) Multiple week interactions between multimodular domains undergo phase transition and form droplets with various sizes. d) Cryo-electron microscope exhibits a ring morphology (Adapted from 3, 21, 22)

In addition, several recently published studies revealed that the LCSs alone or in concert with RNA undergo liquid-liquid phase separation (LLPS), where different physical states with different morphologies are formed. LLPS is modulated by many variables including increased protein concentrations²², posttranslational modifications^{23,24}, decreased temperature²⁵, environmental crowding²⁶⁻²⁸, decreased salt counter ions²⁹ and RNA^{22,30}. Numerous studies have highlighted the contribution of long-range (the electrostatic interactions), and the short-range interactions, as driving force for phase separation. In long-range interactions, charged motifs interact with each other, as in the case of the P-granule disordered protein LAF1³⁰ and the RNA binding protein DDX4²⁵. In addition, DDX4 undergoes short-range interactions, where the blocks of aromatic residues, namely Phenylalanine (F) and Tyrosine (Y), interact with the positively charged Arginine (R). Furthermore, the FUS protein undergoes directional short-range π - π stacking interactions, between F residues, as well as dipole-dipole interactions between the G residues (**Figure 1.3**)^{31,32}.

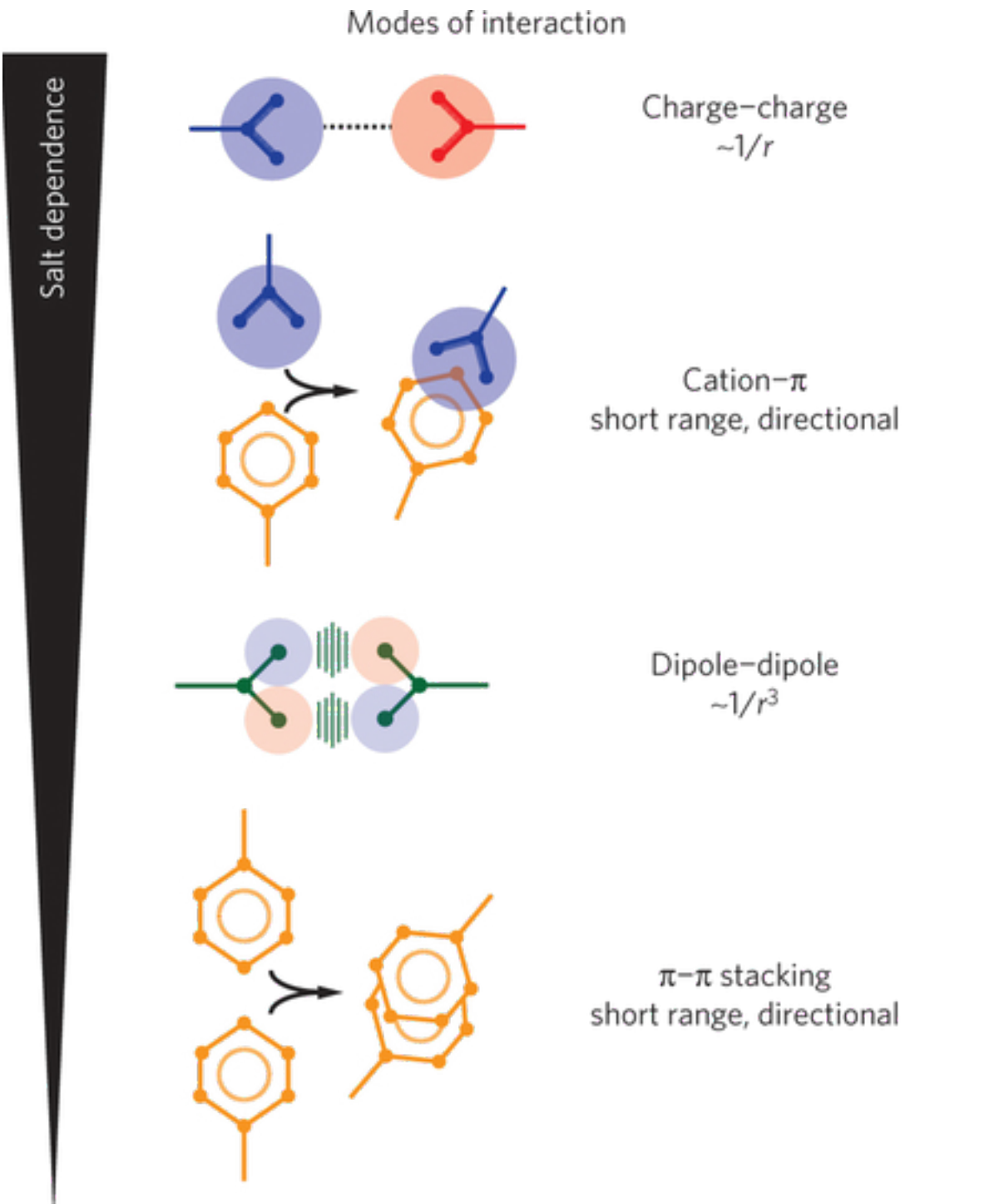


Figure 1.3 Different types of interactions that trigger liquid-liquid phase separation

Long-range interactions, the electrostatic interactions, and short-range interactions, namely cation- π , π - π and dipole-dipole, were found the essence of liquid-liquid phase separation (Adapted from 31)

For decades, RNA was considered as a decoder for genetic information. However, recently the polyanionic nature of RNA was found either to trigger or to prevent the formation of liquid droplets and to have an impact on the physical properties of these droplets. Under which circumstances RNA could perform either role is still enigmatic. For instance, RNA decreases the viscosity of the P-granule disordered protein LAF1³⁰. On the other hand, the viscosity of the Whi3 protein in *Ashbya gossypii* is tunable by RNA depending on the transcripts involved and on their concentration. The protein Whi3 contains an expanded stretch of Q residues and binds to two distinct mRNAs, CLN3 and BNI1. Depending on the mRNA identity, Whi3 protein forms two distinct organizations with different viscosities, fusion event and exchange rate with the bulk²². In addition to the previously mentioned function of RNA, it was also found that RNA delays the “aging” event of Whi3 proteins, in which the protein undergoes a conformation change, which is reflected by the transition from liquid to gel states²². The gel-like state is usually associated with the pathogenic state, the fibrous conformation. However, the liquid state or the phase separation that the protein undergoes is not an obligatory intermediate for fibrillization. For instance, hnRNPA1 can form fibrils without going through the liquid state^{33–35}.

Ultimately, the liquid states have different component rearrangements, where the components of the liquid state can easily reshuffle, while the degree of freedom of the solid-state component is low and the component reshuffling is slow. For instance, water undergoes phase transition to form a liquid state with different physical properties to the solid state. At present, the arrangement of the primary sequences that triggers either gel-like or droplet state is still enigmatic. In particular, the structure-function relationship of macromolecule assemblies that can undergo phase transition is poorly understood. For instance, the cytoplasmic bodies in yeast namely stress granules and P-bodies possess different physical states. The former was found to have a gel-like state while the latter possess liquid states³⁶. In this study, our first aim was to understand whether prion-like proteins containing the LCS PolyQ/N undergo phase transitions and to determine chemical and physical factors that stimulate or trigger phase separation (liquid-solid transition or liquid-liquid phase separation). We chose as a tool, the prion like protein Hrp1.

1.2 The Prion like protein Hrp1 forms visible aggregates

The protein Hrp1 is an mRNA binding protein, containing two RRM domains and a PolyQ/N stretch at its N-terminus and an RGG Box at its C-terminus. It is involved in RNA metabolism³⁷. More precisely, it is implicated in 3' end processing event, such as cleavage and polyadenylation³⁸. It shuttles between the nucleus and the cytoplasm, and contributes to the export of mRNA³⁹. Hrp1 is posttranslationally modified by methylation of the Arginine residues within the RGG box, which affects protein-RNA or protein-protein interactions or the stability of the protein⁴⁰.

Hrp1 was found by Alberti *et al.* (2009), to be a prion-like protein candidate containing the prion-forming domain PolyQ/N. It forms dynamic visible aggregates, which dissolve upon treatment with low concentrations of detergent, namely 2% SDS and binds to thioflavin T dye over time, suggesting that it ages to form fibrils. (**Figure 1.1**, Hrp1 is highlighted in red)¹¹.

Moreover, Hrp1 is implicated in the assembly of stress granules in yeast and is considered as a core component of these cytoplasmic structures^{4,41}. In yeast, non-translated mRNAs could be recruited to these RNP-granules. P-bodies act as mRNA storage and contain mRNA degradation machinery, while stress granules consist mainly of the translation initiation components, such as, eIF4E, eIF4G, eIF4A, eIF4B, PolyA binding protein, eIF3, eIF2 and the 40S ribosomal subunit⁴². Stress granules are formed by inhibition of translation initiation, coexist with P-bodies and are known to undergo phase separation. A recent paper demonstrated the architecture and the organization of stress granules assembly. Stress granules consist of a stable core, formed by a network of protein-protein interactions that is surrounded by a dynamic shell. ATP influences the dynamic and the assembly of the granule. CCT, RVB and MCM ATPases modulate different steps in granule assembly and disassembly^{43,44}. Stress granules are known to be associated with neurodegenerative diseases, where an increase in the formation of stress granules is observed due to mutations occurring within proteins that cause the disease. For instance, the TDP43 protein associates with stress granules and mutations in TDP43 alter the dynamic of these assemblies^{45,46}. Unlike P-bodies, stress granules possess a solid-like state. However, stress granules aggregate but do not display amyloid features³⁶. The solid-like state of stress granules and the liquid-like state of P-bodies are discernible using the compound 1,6 hexandiol. Unlike P bodies, stress granules do not dissolve in cells treated

with 1,6 hexandiol, suggesting that stress granules have solid-like nature. How and why hexandiol triggers the dissolution of P-bodies and has no influence on stress granules is not yet clear³⁶. It is possible that 1,6 hexandiol disrupts weak interactions in liquid state but has no effect on strong interactions in the solid state. A better understanding of the assembly and the composition of P-bodies and stress granules are necessary to address these issues.

1.3 The P-body is a liquid droplet

Non-translated mRNAs are recruited into mRNP granules that are known as P-bodies or stress granules. More importantly, mRNA degradation competes with translation initiation both of which are triggered by mRNA decapping and shortening of the polyA tail. Moreover, the cap binding protein eIF4E inhibits the decapping factors Dcp2 and Dcp1 *in vitro* and *in vivo*, which are P-body components^{41,42,47-49}.

As processing bodies, P-bodies are cytoplasmic granules that harbour the RNA degradation machinery and mediate translation repression. They contain mainly mRNA and RNA binding proteins with Low complexity domains PolyQ/N, known as prion-like domains. In addition, proline-rich motifs are located either within the LCS stretches or downstream. The proline-rich motifs provide flexibility to multimodular domains (LCS) to undergo multiple promiscuous interactions with their partners^{42,50}. P-bodies consist of sub-complexes of proteins that are responsible for mRNA deadenylation, translation repression, decapping and degradation. mRNA decay occurs by two different pathways. First, shortening the PolyA tail of the mRNA to 12 Adenine nucleotides is mediated by the deadenylase CCR4/Pop2/Not complex, and then the exosome mediates the mRNA degradation in the 3' to 5' direction. Alternatively, the shortened mRNA is decapped by the enzymes Dcp2 and Dcp1 and then degraded from 5' to 3' by the exonuclease, Xrn1. The core components of P-body, which are also known as enhancers for Dcp2 and Dcp1 enzymes, such as Dhh1, Pat1p, Edc3 and the Lsm1-7 complex, affect the decapping factors. For instance, Edc3 and Pat1p binds to Dcp2 decapping factor and increase its activity⁴².

Notably, P-bodies are multicomponent membrane-less organelle, where hundred of proteins are involved in the assembly, however few molecules called the scaffold proteins maintain the structure of these assemblies via protein-protein interactions. However, the composition and the assembly of these collectives are still largely not yet clear. P-bodies in yeast containing

non-translating mRNA are dynamic structure and function during cellular stress. For their formation they depend on the amount of the non-translated mRNA and their size and number alter in response to stress such as glucose deprivation, osmotic stress, exposure to UV and the stage of cell growth. Glucose deprivation leads to rapid inhibition of protein synthesis and inhibition of translation initiation, which results in increase of P-body^{51,52}. It has been suggested that mRNA triggers the assembly of P-bodies, where protein complexes are formed independently in the cytoplasm and then recruited sequentially to the mRNA forming mRNP particles. Consequently, aggregation of mRNP particles via protein-protein interactions forms a larger collective, the so-called P-body. For example, Dcp1/Dcp2/Edc3 or alternatively Dcp1/Dcp2/Dhh1/Scd6 and Lsm1-7/Xrn1/pat1 are recruited to the mRNA in an unknown order. Subsequently the 5' end of the mRNA binds Edc3, Dcp2 and Dhh1 and interacts with Pat1 that binds to the 3' end of mRNA and forms a closed loop. In addition, the aggregation of mRNP particles in P-bodies may be driven by the interaction of the self-interaction domain (Yjef-N) in Edc3 and the C-terminus of Lsm4 that contains a PolyQ/N stretch (**Figure 1.4**)⁴². The organization of these prion-like proteins within P-bodies is not well characterized. However, Fromm *et al.* (2014) were able to reconstitute *in vitro* the liquid phase of P-body core component, such as, Dcp2, Dcp1, Edc3 and pdc1 in *Schizosaccharomyces pombe*. Dcp1 activates the decapping enzyme Dcp2 and the remaining proteins are known to form the scaffold of the processing body. The core is built via a network of promiscuous interactions between the 10 HLM (helical leucine Motif) in Dcp2, Pdc1 and the Edc3-lsm domain. Disruption of these interactions prevents the coalescence of the liquid phase *in vitro*⁵³. Lastly, a study made by Banani *et al.* (2016), shed light on the fundamental rules that determine the composition of the phase separated P-bodies in the cell. RNP particles consist of a scaffold and recruits clients depending on the composition, the stoichiometry and the free sites of the scaffold. The clients are molecules with low valency and are much more dynamic than that of the scaffold⁵⁴.

Finally, mRNA plays a crucial role in the assembly of P-granules. However, the cell contains other electrolytes including DNA, polyamine and polyphosphates that are known to impact the aggregation and disaggregation of numerous protein assemblies. Here, we addressed whether polyphosphate play a role in the assembly of P-bodies in the cell.

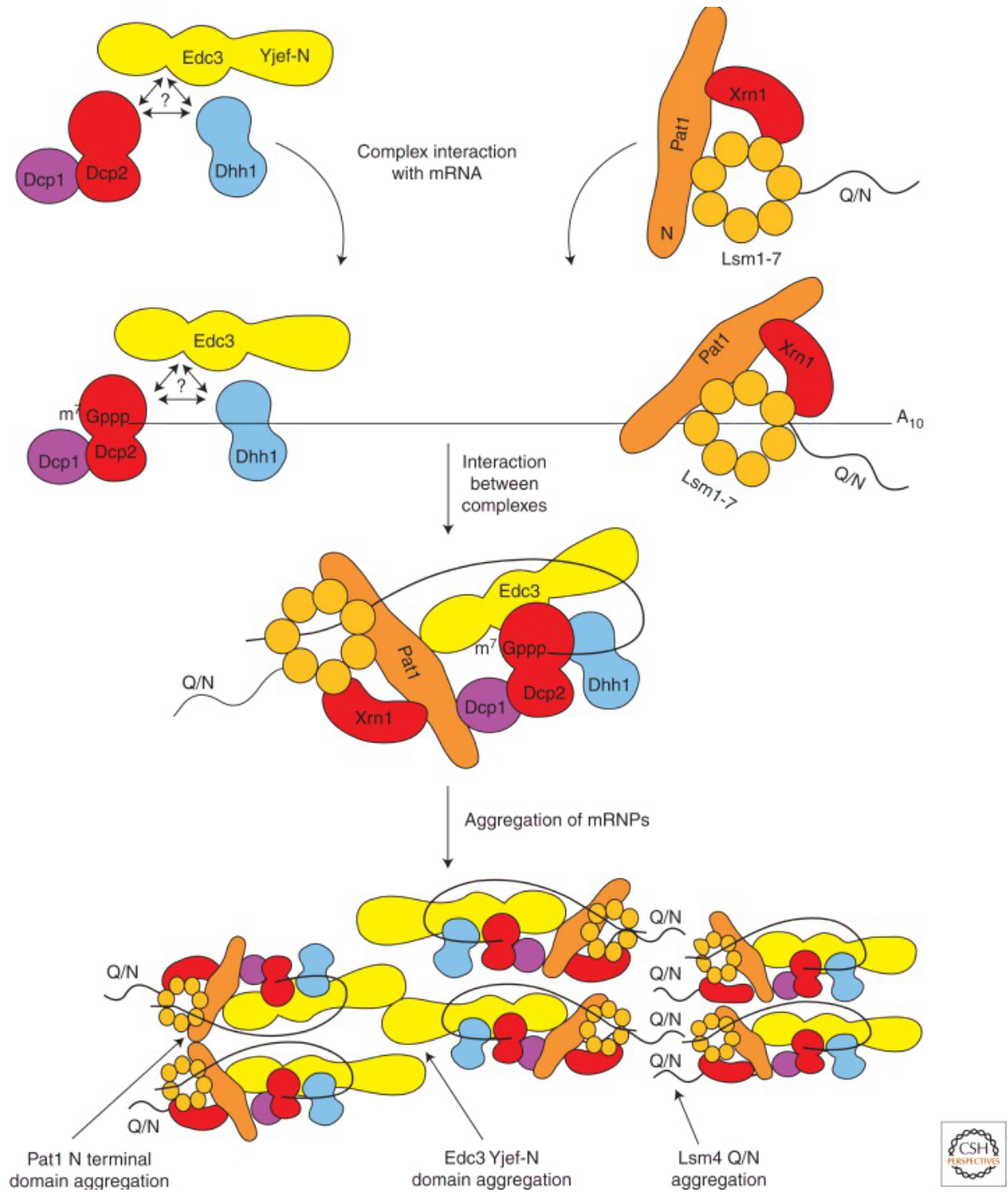


Figure 1.4 Model for P-body assembly

mRNA recruits protein sub-complexes such as the decapping machinery, the translation repression complexes in an unknown order. The core component Edc3 binds to Pat1 and form a loop. And form an mRNP particle. Aggregation of mRNP takes place via LC sequence interactions between Edc3 and Lsm4 (Adapted from 42)

1.4 The role of the multivalent ionic compound polyphosphate in the cell

Polyphosphate (PolyP) are a linear chain of negatively charged phosphorous moieties connected through energy rich phosphoanhydride bonds⁵⁵. They were first discovered in the cytoplasm of the bacterium *Spirillum volutans* as metachromatic granules and were given the name volutin, which were stained pink by a basic blue dye⁵⁶. PolyP are also found in different living organisms such as bacteria, fungi, plants and animals⁵⁷. The chain of PolyP could range from 3 to thousands of residues. Acid-soluble PolyP with a short chain is found at the cell surface, in the periplasm and in the plasma membrane. In bacteria, PolyP are generated by polyphosphate Kinases (PKK1). PKK1 uses ATP as a substrate to catalyze the polymerization of the PolyP chain. It transfers the gamma phosphate group from ATP to generate the negatively charged polymer PolyP. PKK1 is found in various organisms including archaea, fungi and yeast but not in mammals^{58,59}.

PolyP are implicated in distinct biological processes, however, how these are related and the mechanism by which PolyP modulate these biological events are not yet known. For instance, PolyP serve not only as an energy source, but also act as phosphate storage molecules^{60,61}, as a chelator for metal ion such as Ca^{2+} and Mn^{2+} ⁶², as a buffer against alkali ions⁶³ and as a regulator of cellular stress⁶⁴. They also play various roles in many cellular events, such as in gene regulation, in signalling and in proliferation. In *E.coli*, PolyP bind to the Lon protease and form a complex that triggers the degradation of ribosomal proteins. Lon is a protease that is known to bind to DNA and is implicated in the regulation of several cellular events⁶⁵. In addition, PolyP interact with basic positively charged proteins such as histones⁶⁴. For instance, in the bacterium *Caulobacter crescentus*, PolyP interact with the positively charged polyphosphate kinase1 (PPk1). Moreover, in *E.coli* PolyP act as chemical chaperone, where they bind to numerous proteins and protect them against stress. Cellular stress induces aggregation and unfolding of proteins, but once the stress is released, PolyP promote refolding⁶⁶.

It was recently shown *in vitro* that PolyP accelerate the formation of amyloid fibril proteins such as CsgA and α -synuclein in prokaryotes and eukaryotes, respectively. PolyP bind to the amyloid fibrils and alters their seeding capacity, their nucleation propensity and stabilizes the amyloid proteins in their β -sheet conformation. By contrast, PolyP increase the formation of biofilms in pathogenic bacteria and reduce the cytotoxic effect of amyloids in neuronal cells⁶⁷.

In yeast PolyP are synthesized by the vacuolar transporter chaperone (VTC) and accumulates in the extracellular space and in the vacuole^{68,69}. Yeast possesses 4 VTCs, a small transmembrane protein called VTC1 and VTC2, 3 and 4 that have transmembrane domains and a cytoplasmic segment. VTC4 is essential for the accumulation of PolyP in the cell. It produces PolyP from ATP. PolyP in yeast are catalyzed by two exopolyphosphatases, Ppx1 and Ppn1. The latter catalyzes long chains of PolyP and generates a small stretches, while the former catalyzes the end of PolyP and releases orthophosphates (**Figure 1.5**)^{59,60,70}. PolyP in yeast were found to regulate the level of phosphate in the cytoplasm⁷¹. Shirama *et al.* (1996) showed that the phosphate in the cytosol remains constant after 4 h of phosphate starvation, but the PolyP in the vacuole decrease during this time. However, the amount of inorganic phosphate in the cytosol begins to be depleted after 6 h of starvation⁷²⁻⁷⁴. Moreover, PolyP in yeast sequester amines such as Arginine⁷⁵, in the vacuole and acts as cytoplasmic pH regulator.

Importantly, PolyP and inositol pyrophosphate (IP₇) are metabolically linked. IP₇ is generated by *Kcs1*, and deletion of *Kcs1* decreases the amount of PolyP in the cell. However, PolyP have no effect on IP₇⁷⁶. The products of inositol pyrophosphate pathway such as IP₄, IP₆, IP₇ and IP₈ are involved in numerous cellular events such as gene expression, maintaining the telomere length, chromatin remodelling, RNA export and endocytic trafficking⁷⁷⁻⁸⁸. IP₇ and PolyP modify proteins non-enzymatically via post-translational modifications^{86,89}. IP₇ pyro-phosphorylates a Pre-phosphorylated serine, while the poly-phosphorylation takes place on a lysine. For instance, the nuclear signal recognition 1 protein (Nsr1) that is involved in rRNA biogenesis and its interacting partner topoisomerase1 (Top1) in yeast are poly-phosphorylated. The phosphorylation takes place on a lysine residue in the N-Terminal Polyacidic cluster, enriched in Serine (S) and Lysine (K)⁷⁶. Protein modification via

phosphorylation regulates cellular events and signalling pathways, and consequently modulates protein-protein interactions and localization. Regarding the liquid state, it was shown that post-translational modifications such as phosphorylation, could triggers condensation or dissolution of membrane-less organelles^{23,24}. Rosen and co-workers demonstrated that increasing the phosphorylation sites of a peptide, that represent an artificial model of the transmembrane protein nephrin, leads to phase separation²¹. However, the effect of polyphosphate and *Kcs1* on RNA granules assembly is unknown. Hence, I investigated whether PolyP play a role in mediating phase transitions in the cytoplasm.

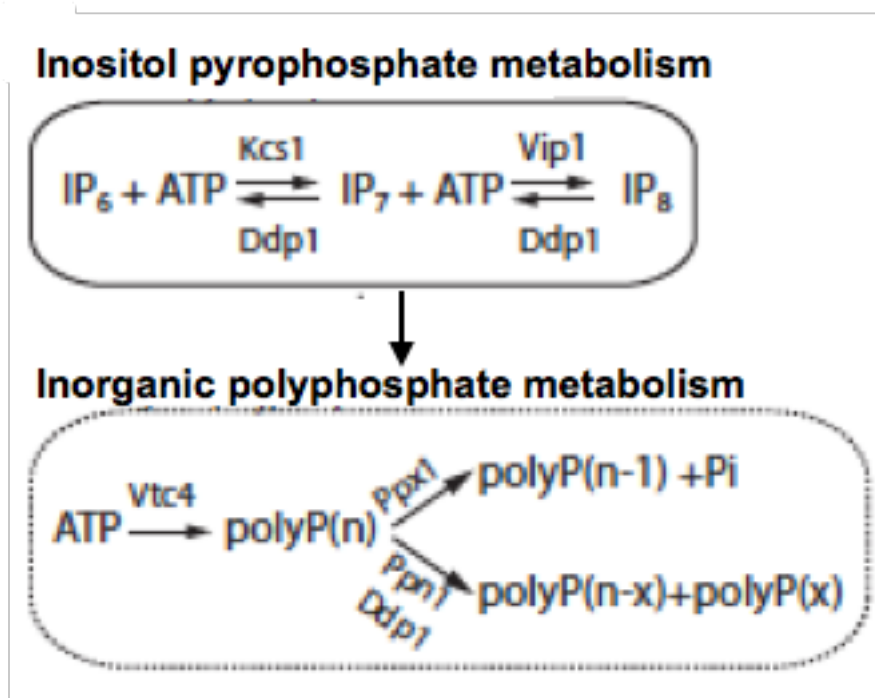


Figure 1.5 Pathway of inositol pyrophosphate and polyphosphate metabolism

1.5 Research project

1.5.1 Problematic and hypothesis

Prion-like proteins containing low complexity domain PolyQ/N are found to form visible aggregates that unlike the traditional known amyloid aggregates, they dissolve under low concentration of detergent¹¹. A study suggests that the LCS has the propensity to aggregate, to polymerize and to form a solid-like state, the hydrogel. The solid-like state was formed under extremely non-physiological condition via homo and heterotypic interactions. Another study proposed an alternative scenario demonstrating that LCSs are able to undergo multiple weak promiscuous interactions resulting the formation of the droplet, via liquid-liquid phase separation mechanism²¹. Regarding the secondary structure of the solid-like state and the liquid-like state, the former was found to form a β -secondary structure with filamentous morphology, while the latter was reported to form coiled-coils with a ring shape.

The study established by Alberti *et al.* (2009), aiming to identify prion-like domain in *S. cerevisiae*, discovered 200 protein candidates with prion-like domain containing LCS-PolyQ/N that form visible aggregates *in vitro*. Among these proteins are mRNA binding proteins that dissolve in the presence of the non-denaturing condition 0.1%T20 and 2% SDS. Moreover, the effect of the thioflavin (Tht) dye is absent or delayed well over 24 hours. One example is the mRNA binding proteins Pop2 and Ccr4, which are components of P-body. In contrast, the mRNA binding protein Hrp1 was found to bind to Tht dye after 0.1 hour, to be retained in 0.1% T20 but to dissolve in low detergent concentration (2% SDS). The properties and the nature of these aggregates were not yet identified. At first, the study established by mcknight *et al.* (2012) claims that LCS forms hydrogel. In contrast, Rosen *et al.* (2012) claims that LCS forms droplets. I initiate my study by hypothesizing that mRNA binding proteins containing LCS form droplets in the cell. As a prove of concept, I chose the mRNA binding protein Hrp1 as an artificial model, first to shed the light on the LCS and their function as a force to generate droplet, and second to solve the conundrum concerning the nature and the organization of the collectives containing LCS *in vitro* and *in vivo*.

In vivo, the assembly of these collectives is triggered by the crowded nature of the cytoplasm²⁶, by the post-translational modifications such as phosphorylation or methylation²⁵, by the protein gradient concentration within the cell⁹⁰ and more importantly by the negatively charged RNA²⁹. Numerous studies have shown that the RNA could trigger or inhibit the assembly of the droplet in the cell. More importantly, the polyelectrolyte RNA was shown to dictate the biophysical properties of these assemblies. It is not surprising, that the polyelectrolyte RNA plays a crucial role in the assembly of the liquid matter in the cell and is most likely the driving force for droplet condensation. The multivalent ion salts, the negatively charged/positively charged polyelectrolytes are used in the industry to coalesce and flocculate colloids in order to clarify wastewater. Moreover, they are also used to change the biophysical properties of the polymer-based colloids or so-called smart materials that have applications in drug delivery, sensor design and smart emulsifiers⁹¹.

Similarly, the cell uses biopolymers to organize membrane-less organelles. The cell contains a variety of biopolymers such as RNA, DNA, polyamines and polyphosphates that are known to influence the aggregation and disaggregation of numerous protein assemblies. For instance, the polyamine, spermidine, is known to condense the DNA and to trigger the aggregation of distinct proteins such as polyglutamine (PolyQ) protein, α synuclein, and the F-actin^{92,93}. It was reported that spermidine triggers the aggregation of F-actin, while the nucleoside phosphates disassemble the aggregation. The negatively charged phosphates could act as an antagonist to the positively charged amines in inducing protein condensation⁹⁴.

Based on an initial study, I demonstrated that the prion like protein Hrp1 containing LCS PolyQ/N forms droplets in the presence of negatively charged polyelectrolyte such as polyacrylic acid. In addition, ample of studies have shown the formation of protein droplets containing LCS *in vitro* in the presence of the negatively charged polyelectrolyte, the RNA. Hence, I hypothesized, that the negatively charged polymer under which Hrp1 forms droplets could mimic the negatively charged polyelectrolyte such as RNA, DNA and PolyP in the cell. Based on these observations, I proposed to explore the potential and the universal role of the highly abundant polyelectrolyte PolyP as a regulator in the condensation/dissolution of membrane-less compartment forming liquid droplet in the cell initiating with the P-body, knowing that P-bodies consists of mRNA binding proteins containing LCS and possess liquid nature *in vivo*.

1.5.2 Objectives

To obtain insights into whether prion-like proteins undergo liquid-solid or liquid-liquid phase separation, whereby a gel-like material or a droplet develops respectively, I chose the prion-like protein Hrp1 as a model. Specifically I investigated:

- Whether the purified Hrp1 undergoes phase separation under different chemical conditions that trigger the formation of droplets using a high-throughput screen.
- Whether the prion-like domain (PrD) or the RRM of Hrp1 is responsible for the phase separation under the same conditions.

We found that the PrD alone formed a gel-like material that has a cross- β secondary structure. In contrast, another study, suggests that PrDs form droplets via multiple weak interactions that are mediated by coiled-coil secondary structure. Hence, I investigated the secondary structure and the morphology of Hrp1 full-length protein and its PrD domain using Circular Dichroism (CD) and Transmission electron microscopy (TEM).

Recent studies have shown that the negatively charged RNA triggers formation of droplets by phase-separation. Notably, I found that negatively charged polyelectrolytes, which promotes the formation of Hrp1 droplets, mimics RNA and I hypothesized that the highly abundant polyelectrolyte PolyP regulate P-body formation via phase separation and investigated:

- Whether depletion of phosphate has an effect on P body formation
- Whether depletion of PolyP from the cell would prevent P-body formation
- Whether PolyP colocalize with P-bodies in the cytoplasm

1.5.3 The techniques used in this study

In this Study different techniques were used to investigate the potential role of PolyP in P-body formation. First to investigate whether prion-like proteins undergo phase separation, the

protein of interest Hrp1 was purified via affinity chromatography using NI-NTA column and Size Exclusion Chromatography (SEC). I then tested for phase separation under a variety of conditions, including the presence of polyelectrolytes. Subsequently, using light microscopy, I monitored the formation of droplets. To obtain insights on the organization and the conformation of the heterogeneous matter within the droplets, Circular Dichroism (CD) and Transmission electron microscopy (TEM) were performed on the purified proteins Hrp1 and its PrD domain.

After elucidating the conditions under which Hrp1 protein forms droplets. I verified whether PolyP have an effect on the condensation and dissolution of P-bodies. Specifically, I determined whether PolyP affect the number and size of P-bodies labeled with mCherry Edc3 using fluorescence microscopy.

2 Materials and Methods

2.1 Media

For protein overexpression, *E.coli* BL21 (De23) was cultured in terrific Broth media (TB) containing 12 g/l of tryptone, 24 g/l yeast extract and 4 ml glycerol in addition to a salt solution separately autoclaved consisting of 0.17 M KH_2PO_4 and 0.72 M K_2HPO_4 .

For the phosphate and glucose deprivation experiment, synthetic media was mainly used. The composition of synthetic media was 0.17 % yeast Nitrogen base, 0.5 % ammonium sulphate, 2 % glucose and amino acid.

For phosphate depleted synthetic media, the phosphate was precipitated using 1 M MgSO_4 with high concentrated ammonium hydroxide and kept at RT for 30 min followed by a filtration.

2.2 Strains and Plasmids

In this study, bacteria and yeast strains as well were used. DH5 α and BL21 (De3) were used for cloning and for protein expression of Hrp1 and its variants, respectively. On the other hand, the yeast strains BY4741-mcherry Edc3 and BY4741-mcherry Edc3-*vtc4* Δ were used for P body analysis.

Table 2.1. Bacterial and yeast strains

Strain	Genotype	Reference
DH5 α	F ⁻ Φ 80 <i>lacZ</i> Δ M15 Δ (<i>lacZYA-argF</i>) U169 <i>recA1 endA1 hsdR17</i> (rK ⁻ , mK ⁺) <i>phoA</i> <i>supE44</i> λ - <i>thi-1 gyrA96 relA1</i>	Common laboratory strain
<i>E.coli</i> BL21(De3)	B F ⁻ <i>ompT gal dcm lon hsdS_B</i> (<i>r_B⁻m_B⁻) λ(DE3 [<i>lacI lacUV5-T7p07 ind1 sam7 nin5</i>]) [<i>malB⁺</i>]_{K-12}(λ^S)</i>	Common laboratory strain
BY4741	MATa <i>his3</i> Δ 1 <i>leu2</i> Δ 0 <i>met15</i> Δ 0 <i>ura3</i> Δ 0	Common laboratory strain
BY4741-mcherry Edc3	MATa <i>his3</i> Δ 1 <i>leu2</i> Δ 0 <i>met15</i> Δ 0 <i>ura3</i> Δ 0: <i>hph^R</i>	Jacqueline Kowaryk

BY4741-mcherryEdc3- *vtc4*Δ

MATa his3Δ1 leu2Δ0 met15Δ0 ura3Δ0:nat-
1^R

In this study

The used plasmids were either for protein expressions *in vitro* namely Hrp1 and its variants or to delete the gene that is responsible for PolyP synthesis *vtc4*. For this purpose, pet24d(+) and PAG25 as well were utilized, respectively.

Table 2.2. Plasmids for protein expressions and gene deletion

Plasmids	Genotype	Reference
Pet24d (+)	Protein overexpression	Dr. Christian Baron
PAG25	Cassette containing the selection marker CloNat to delete the gene of interest via homologous recombination	Common laboratory plasmid

2.3 The designed primers for different experiments

Primers were designed to amplify the genes of interest namely Hrp1 and its variants from yeast genomic DNA and Hrp1 plasmid construct, respectively. Hrp1 and RRM fragment were amplified using PCR, whereas the PrD was amplified via SOE-PCR.

Moreover, primers were designed to delete *vtc4* gene using PAG25 as a template and to perform a diagnostic PCR in order to confirm the successfulness of the deletion.

The red highlighted sequences are the restriction enzyme sites.

Table 2.3. PCR primers for *in vitro* and *in vivo* studies

Primers	Forward (5' → 3')	Reverse (5' → 3')
<i>Hrp1</i>	CGGCGTACGAGCTCTGACGAA GAAGAT	CGCGGATCCTTACCTATTATATGGAT GGTAGCCATT
PrD-Fragment 1	CGGCGTACGAGCTCTGACGAAGA	ATGTCTTGGCTCAGCAGACAAATCCG

	AGAT	CTTT
PrD –Fragment2	AAAGCGGATTTGTCTGCTGAGCCA	CGCGGATCCTTACCTATTATATGGAT
	AGACAT	GGTAGCCATT
Hrp1-RRM	CGGCGTACGAAAGAAAGTTGCAA	CGCGGATCCTTATCTCTTGATTTCGAT
	GATG	
<i>Vtc4</i>	GCTAACAAATCAAATCGGCCAATAA	TTATTACTTAATTATACAGTAAAAAA
	AAGAGCATAACAAGGCAGGAACA	AACACGCTGTGTATTTTCGACACTGGA
	GCTAGATCTGTTTAGCTTGCCTTGT	TGGCGGCGTTAG
	CCCCG	
<i>Vtc4</i> -diagnostics primers	CCAGATGCGAAGTTAAGTGC	CGCCTGGTGAAGGTGTGC

2.4 Extraction of yeast genomic DNA

The yeast By4741 was grown overnight in 10 ml YPD media (1 % yeast extract, 2 % peptone, 2 % dextrose) at 30°C and 250 rpm to saturation. The cells were harvested by centrifugation at 4000 rpm for 5 min. The supernatant was removed, the pellet was re-suspended in 500 µl distilled water and centrifuged at 13 000 rpm for 30 sec.

For cell disruption, 200 µl of Lysis buffer (2 % Triton X-100, 1 % SDS, 100 mM NaCl, 10 mM Tris pH 8 and 1 mM EDTA), 200 µl of Phenol chloroform and washed glass beads were added to the pellet. The latter was lysed by vortexing about 3 to 5 times for 1 min each and kept for 1 min on ice in between the vortexing events. Subsequently, 200 µl of TE buffer (10 mM Tris pH 8 and 1 mM EDTA) was added and the lysate was clarified via centrifugation at 13000 rpm for 5 min. To precipitate the DNA, 1 ml of 100 % Ethanol was added to the supernatant and inverted allowing mixing. Next, it was centrifuged for 2 min at 13000 rpm, re-suspended in 400 µl TE buffer containing 30 µg of RNaseA and incubated at 37°C for 30 min. Furthermore, 10 µl of 4 M Ammonium acetate and 1 ml of Ethanol was added to the sample and then placed at – 20°C for 30 min to allow precipitation. Ultimately, the sample was centrifuged, air-dried and re-suspended in 30 µl TE buffer.

The extracted genomic DNA was verified or detected by electrophoresis on 1 % agarose gel in TAE buffer (40 mM Tris-acetate, 1 mM EDTA, pH 8.2).

2.5 Overexpression and purification of Hrp1 and its variants

The gene encoding for Hrp1 Protein was amplified via PCR using extracted yeast genomic DNA. The amplified fragment was inserted in Pet24d (+) plasmid containing His-Tev Tag. In contrast, RRM and PrD were amplified via PCR and SOE-PCR respectively, using Hrp1 construct as a template. Similar to Hrp1, these fragments were also inserted in Pet24d (+).

The proteins of interest were all overexpressed in *E.coli* BL21 (De3) with 1 mM IPTG for 4 hours (hrs) at 37 °C and 300 rpm. The cells were harvested via centrifugation at 15000 rpm for 20 min and re-suspended in binding buffer containing 5-10 mM imidazole (20 mM Tris pH8, 500 mM NaCl and protein inhibitor cocktail). Subsequently, the cells were disrupted using the French-Press for two cycles followed by a centrifugation at 15000 rpm for 30 min. The supernatant was filtered and then loaded on 4 ml Ni-NTA packed resin. The column was washed with 5-column volume (CV) of binding buffer and the bound proteins were eluted stepwise from the resin using the elution buffer consisting of 500 mM imidazole (20 mM Tris pH8, 500mM NaCl).

The protein fractions were pooled together and dialyzed against the TEV protease enzyme buffer (10 mM Tris pH 8, 125 mM NaCl and 5 mM DTT). The dialysis was performed for 4 hours using the dialysis membrane and by changing the buffer hourly. Subsequently, the protein was treated with Tev-protease enzyme at RT for overnight. For the digestion reaction, 3 ug of protein were treated with 1 Unit (U) of enzyme. In order to verify whether the His-tag was cleaved, a 10 % of SDS-PAGE was performed.

The cleaved protein was dialyzed against equilibration buffer (20 mM Tris pH 7.5, 200 mM NaCl and 0.5 mM EDTA) and loaded on Size Exclusion Chromatography (SEC) to separate the protein of interest from the contaminants. The purified protein was concentrated with Amicon Ultra Centrifugal filters and stored at -80°C for further manipulation.

The purity of the purified proteins was verified via SDS-PAGE and the concentration was accessed using The BSA assay.

2.6 Circular Dichroism Spectroscopy

For CD spectroscopy analysis, Hrp1 and PrD were dialyzed against a buffer (50 mM NaCl, 20 mM phosphate buffer pH 7.5), followed by protein quantification using the BSA assay. The proteins of interest were diluted to the desired final concentration (2.5 μ M) and the CD spectra were acquired using Jasco J810. The ellipticity of the proteins was measured in 0.2 cm quartz cuvette from 195 nm to 260 nm at different temperatures (4°C, 20°C and 75°C).

The molar ellipticity $[\Theta]$ was calculated using the following formula;

$$[\theta](\text{deg} * \text{cm}^2 * \text{dmol}^{-1}) = \frac{\theta_{\text{obs}}(\text{mdeg})}{10 * c \left(\frac{\text{mol}}{\text{L}}\right) * l(\text{cm})}$$

Where Θ is the observed ellipticity obtained from the instrument, c is the concentration of the protein and l is the quartz cuvette diameter.

The obtained spectra were smoothed and corrected against the buffer and the secondary structure of the protein was determined using the ContinLL algorithm obtained from the Dichroweb website, which allows an online analysis of CD spectra.

2.7 Transmission Electron Microscope analysis

For TEM analysis, different protein concentrations were prepared from (1mg/l - 10 mg/ml), where 5 μ l of the samples were loaded on a carbon-coated grid for 5 min at RT. Subsequently, the excess of liquid was removed using filter paper and then negatively stained with 2 % Uranyl acetate. Finally, the imaging was performed using Philips Tecnai 12 (Eindhoven, The Netherland), operated at 80 KV.

2.8 Design a cassette for homologous recombination to replace the gene to be deleted with an antibiotic as a selection marker

The cassette for homologous recombination was prepared by amplifying the antibiotic selection marker Clonnat via PCR using the plasmid PAG25 as a template. The designed primers for the PCR were flanked with the 5'UTR and 3' UTR of the gene to be deleted.

2.9 Homologous Recombination

Homologous recombination was carried out by first preparing competent cell of the strain, where the designed cassette will be transformed. Hence, a single colony of the strain of interest was inoculated in 5 ml YPD and incubated overnight at 30°C and 250 rpm. The next day, the optical density (OD) of the culture was determined by spectrophotometer at a wavelength of 600 nm and diluted in 50 ml of YPD media to an OD₆₀₀ of 0.1. It was kept to grow at 30°C and 250 rpm until an OD₆₀₀ of 0.4-0.6 is reached. The cells were collected by centrifugation at 4000 rpm for 5 min and the pellet was re-suspended and washed twice with 25 ml of distilled water. Next, the pellet was re-suspended with 1 ml of distilled water and centrifuged at 4000 rpm for 1 min. The supernatant was removed and again 1 ml of distilled water was added and aliquots of 100 µl were prepared for the transformation.

The prepared cell aliquots were centrifuged at 13000 rpm for 1 min, the supernatant was discarded and the transformation mix ((PEG 3350 (50 % (W/v)), Lithium Acetate 1 M, single stranded carrier DNA (2 mg/ml) and sterile water) was added. 8 µl of the amplified cassette was added to the competent cells in the presence of the transformation mix and re-suspended vigorously by vortexing. Subsequently, the tubes were incubated at 42°C in a water bath for 40 min and then centrifuged at 13000 rpm for 1 min. The cells were then re-suspended by vortexing vigorously after addition of 1 ml YPD and incubated at 30 °C for 2-3 hours. Finally, the cells were plated on YPD media containing the appropriated antibiotic selection marker and kept at 30°C for 2-3 days.

To verify whether the homologous recombination was successful and consequently the gene of interest was deleted, a diagnostic PCR was performed on the colonies that grew on the plate with the appropriate selection marker. To carry out the diagnostic PCR, single colonies were picked, dissolved in 20 µl of sterile water and incubated at 99°C for 15 min and 30 sec. Subsequently, the aqueous layer was used as a template to run the PCR and the primers were designed in a manner that bind to the genome and to the selection marker that replaced the gene of interest.

2.10 Observation of P-bodies in mid-log glucose starved cells

In this study, the P body formation was studied in BY4741-mcherry Edc3 and in BY4741-mcherry Edc3-*vtc4Δ*, depending on the experiment to be performed.

To study the P body formation, the strains were grown in 5 ml complete synthetic media at 30°C and 250 rpm to saturation, and then diluted in 50 ml synthetic media to an OD₆₀₀ of 0.1. The latter was allowed to grow till an OD₆₀₀ of 0.3-0.4. The 50 ml culture was split in two and washed twice at 3000 rpm for 3 min with either a complete synthetic media that serve as a negative control for P body induction or with synthetic media lacking glucose that induces P body formation. Next, the cultures were re-suspended in synthetic media with and without glucose and kept for 15 min at 30°C and 250 rpm. At last, imaging was performed using Nikon TE200U. For imaging, wells of a multiwell Matriplate were coated with concanavalin A (ConA). The ConA enables the cells to gently adhere the surface of the well.

Con A was left for 15 min at RT in the well, removed and then washed with distilled water. Afterwards, ConA was activated by addition of 20 mM MnSO₄ and 20 mM CaCl₂ and incubated for another 15 min. The activation of ConA through cooperative binding of the metal ions Ca²⁺ and Mn²⁺ enables cell fixation, whereby ConA binds to the cell surface. The solution was then removed and the wells were washed with distilled water.

In order to detect the P-body, Edc3 the core component of the P-body was tagged with mCherry. It was visualized at an exposure time of 100 ms and by performing a Z stack with a step size of 0.6 μm using the Nikon TE 200U Microscope. For statistical analysis almost 100 cells were analyzed using the software ImageJ 64.

To note, for the co-localization experiment of P body and PolyP, the cells were starved for 30 min instead of 15 min due to the incubation time of DAPI^{73,95}. Based on the fluorescence scanning experiment Dapi was visualized using YFP filter.

2.11 Detection of PolyP with DAPI staining using the fluorometer

The wild type BY4741-mcherry Edc3 and BY4741-mcherry Edc3-*vtc4Δ* were grown in 5 ml complete synthetic media at 30°C and 250 rpm. It was diluted in 50 ml synthetic media to an OD₆₀₀ of 0.1 and kept to grow under the same condition.

To detect PolyP in living cells, DAPI fluorophore was used, where the cells were incubated with 10 µg/ml of DAPI and kept at 30 °C for 30 min. Afterwards, the cells were gently washed twice at 3000 rpm for 2 min and re-suspended in synthetic media.

The fluorescence of PolyP were followed at different OD₆₀₀ and the fluorescence excitation and emission was acquired using the spectrofluorometer, SpectraMaxGEMINIXS. The fluorescence spectra were obtained by exciting the sample at specific wavelength and by scanning the emission between 400 nm and 600 nm. The bandwidth between the excitation and emission is about 50 nm. For the fluorescence measurement, it is noteworthy that the cells were consistently diluted to an OD₆₀₀ of 0.2 to avoid saturation of light diffraction.

2.12 P-body analysis and quantification of number and size

The average number of of P-bodies per cell was analyzed using the Image J software, where a maximal projection was performed on the obtained Z stacks, followed by processing the image using the find maxima tool. The obtained maxima, which are the P-bodies, were re-directed to the selected or segmented cells and the foci number per cell were measured. This method determines the number of P-bodies in each segmented cell.

Another analysis was performed to quantify the number of the P-bodies, where Otsu thresholding was used. A maximal projection was carried out, the image was smoothed and the background was subtracted. Next, the image was converted to 8-bit and Otsu thresholding was performed. The LUT was inverted and the particles were analyzed using analyse particle tool. The measurements were re-directed to the original file. Finally, a table containing information concerning the area (pixel²), the mean intensity and the sum of pixel is obtained. The area in nm² was calculated given every Pixel is 0.43 nm for a total magnification of 150. Consequently, the radius was calculated assuming a spherical P-body area where;

$$A = \pi r^2$$

To note, the detection was performed using an objective of 100x with 1.5 magnifier resulting a total enlargement of 150.

$$\text{Cell size per pixel} = \frac{\text{Physical length of a pixel on a CCD camera}}{\text{Total magnification}}$$

2.13 Statistical analysis

The Phosphate and glucose deprivation experiment were done in triplicate. The statistical analysis was performed using the Student t-test and Mann-Whitney U-test for population analysis. A P value of less than 0.05 was considered to illustrate a statistical significance. The used softwares for the statistics were Excel, Graphpad prism and R.

3 Results

3.1 Polyanionic molecules induce liquid-liquid phase separation of the RNA binding Protein Hrp1 *in vitro*

To investigate whether prion-like proteins containing the LCD PolyQ/N form droplets, the RNA binding protein Hrp1 was selected as a model. Recently, Hrp1 was reported to form visible aggregates, to bind to ThT (Thioflavin) dye and to dissolve in the presence of 2 % SDS¹¹. However, the nature and the physical properties of these aggregates were not previously known. Hence, the purified Hrp1 was subjected to varieties of conditions and then screened for droplet formation. The scheme of the procedure is summarized in Supplementary Figures (**Fig.S 7.1**).

Hrp1 was purified via affinity chromatography using the NI-NTA column followed by Size Exclusion Chromatography (SEC) for further purification. Hrp1 was expressed in BL21 (De3) and eluted at 60% imidazole during NI-NTA purification (**Figure 3.1.a**). To rule out the possibility that droplet formation is hindered or induced by the His-Tev-Tag, the tag was cleaved with TEV-protease overnight at RT (**Figure 3.1.b**). Next, SEC enabled the separation of Hrp1 protein from the remaining contaminant proteins that have similar affinity to the NI-NTA column (**Figure 3.1.c**). Consequently, a pure protein was obtained. However, Hrp1 protein was found to migrate at higher molecular weight (MW) (~75 KDa) than expected (~59 KDa, as reported in SGD) (*Saccharomyces* Genome Database).

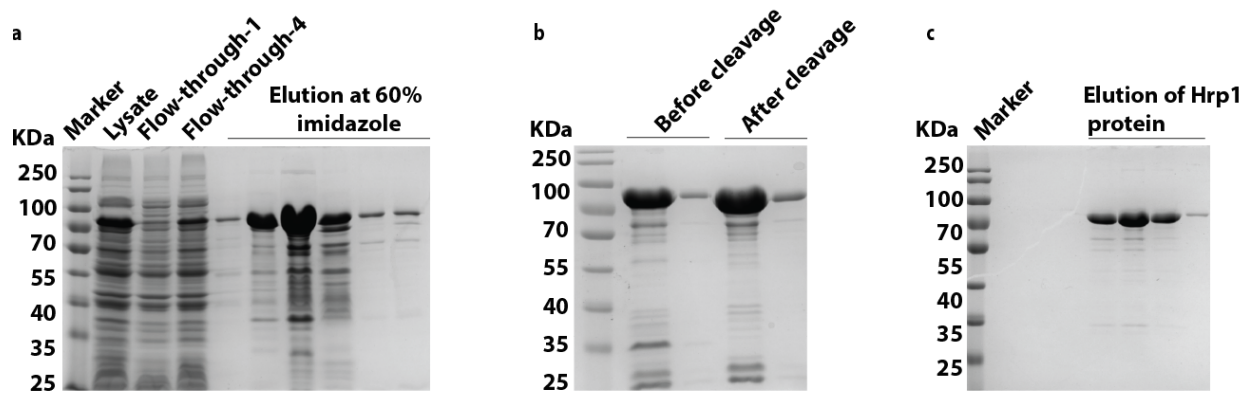


Figure 3.1. Hrp1 purification approach

a) Hrp1 protein expression and NI-NTA purification step. The lysate of Hrp1 was subjected to a pre-packed 4 ml NI-NTA column. The protein of interest was eluted with 60% imidazole, which is equivalent to 300 mM imidazole. b) Cleavage of His-tev tag from Hrp1 using Tev protease enzyme. Lanes 2 and 3 represent the pattern of two different concentrations of Hrp1 before cleavage and lanes 4 and 5 represent the pattern after cleavage. The difference of MW band migration before and after cleavage is approximately 1 KDa. c) Secondary purification of Hrp1 using SEC. Hrp1 was loaded on SEC to remove the contaminant proteins

Purified Hrp1 protein ($\sim 400 \times 10^{-6}$ mole) was subjected to a screen of 96 different conditions, including various polymers, salt and buffer concentrations. Bovine Serum Albumin (BSA) protein was used as control, since its secondary structure is known to consist of 60% helices. Droplet formation was monitored by light microscopy.

The conditions under which the protein was tested were clustered based only on the polyelectrolyte types, assuming that the polyelectrolyte mimics both the crowded environment of the cytoplasm and the negatively charged biopolymers within the cell (**Figure 3.2.a** and **Fig.S 7.3**. (See the detailed conditions)). Hrp1 protein undergoes phase separation and forms droplets of different sizes only in the presence of negatively charged polyelectrolytes, namely polyacrylic acid and its derivatives. By contrast, in other polyelectrolytes, Hrp1 forms precipitates. In particular, the protein precipitated in the polyamine, Jeffamine (**Figure 3.2.a**). The BSA control did not form any droplets under the negatively charged conditions, polyacrylic acid sodium salt and its derivatives.

It has been suggested that LLPS (Liquid-Liquid Phase separation) is concentration-dependent, where it is triggered by an increase in the local protein concentration⁹⁶. For instance, stress granules are formed in a concentration dependent-manner³⁴. Hence, we titrated the amount of Hrp1 in the negatively charged condition, poly acrylic acid sodium salt, and found that the protein forms larger and clear droplets as the concentration increases (**Figure 3.2.c**).

To examine whether LCD or the RRM drives the phase separation of the protein, the PrD and the RRMs of Hrp1 were separately purified and treated under the same conditions as stated above for the Hrp1 full-length protein (**Fig.S7.2**). As expected, PrD and the RRM form precipitates (**Figure 3.2.b**). These results suggest that both the RRM and the LCD are necessary for the formation of Hrp1 droplets. Remarkably, during the purification of the PrD, a solid-like state (gel-like material) formed when PrD was incubated with Tev-protease enzyme overnight at RT (**Fig.S 7.1**). The solid-like state was sensitive to temperature and dissolved with increasing temperature (data not shown).

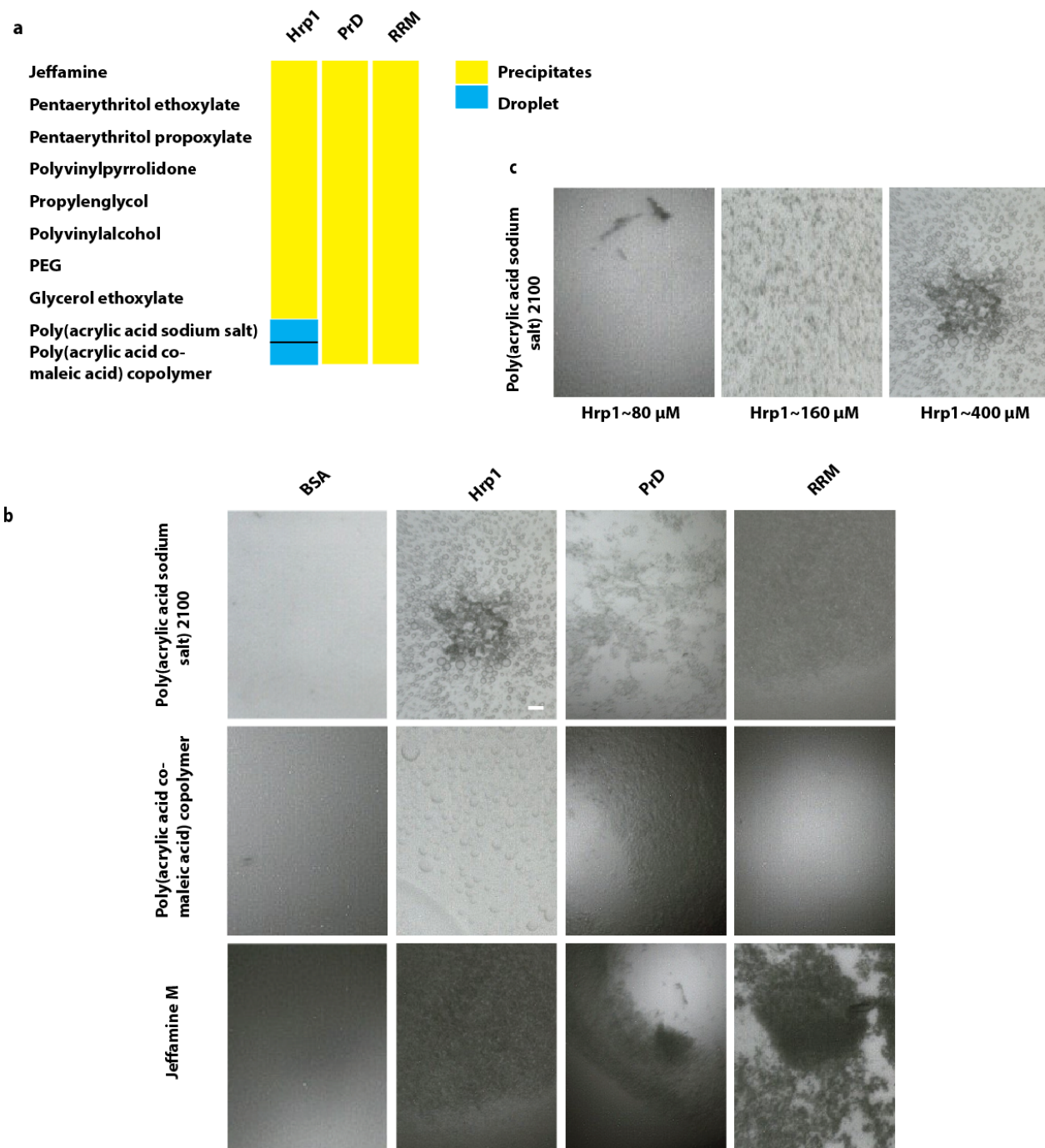


Figure 3.2. Induction of Hrp1 droplets is a concentration-dependent and sensitive to polyanionic molecules

a) Global analysis of the screening under which Hrp1 forms droplets. The polymers were clustered assuming that the polymer first mimics the crowded environment of the cytoplasm, and, second that it tunes the protein-protein interactions, without taking into consideration the salt, the pH and the buffer used. b) Hrp1 under the negatively charged conditions such as poly acrylic acid sodium salt and polyacrylic acid co-maleic acid copolymer forms droplets of different sizes. In the presence of a positively charged polymer, such as, Jeffamine M, Hrp1 forms precipitates. In contrast, the PrD and the RRM form different kind of precipitates depending on the polymer used. c) Increasing the concentration of Hrp1 under poly (acrylic acid sodium) salt leads to clear droplet formation

3.2 Hrp1 is largely in an alpha helical conformation

The crystal structure of Hrp1-RRM was resolved in 2006, and was shown to exhibit 25 % of helical secondary structure and 26 % of β -sheets³⁷. In this study, the secondary structure of the full-length protein was analysed using CD spectroscopy (**Figure 3.3.a**). The CD spectra of Hrp1 both at 4°C and at 20°C display two minima, namely at ~ 208 nm and 222 nm, while at 75°C, the protein exhibits one minimum at ~ 200 nm (**Figure 3.3.a**). Based on the ContinLL algorithm⁹⁷, the protein consists predominantly of helical secondary structure and becomes unstructured with increasing temperature above 20°C (**Figure 3.3.b**). At 4°C and 20°C, almost 29 % of the protein forms helices, which are lost at 75°C. Instead, at 75°C the protein consists mainly of disordered structures. Attempts were performed to study the secondary structure of the PrD, however this was unsuccessful mainly due to protein precipitation in the cuvette. The PrD protein solution became turbid and opaque overtime. Therefore, it was not feasible to compare the conformation of the full-length protein and the PrD, and consequently study the contribution of the critical amino acids towards the formation of the secondary structures and droplet formation *via* point mutations. TEM analysis was performed to elucidate the morphology of the full-length protein and PrD forming droplets or the gel-like material, respectively.

TEM analysis of full-length Hrp1, unlike the elongated morphology of Hrp1-PrD, displays a spherical morphology and filamentous morphology as well (**Figure 3.3.c and d**).

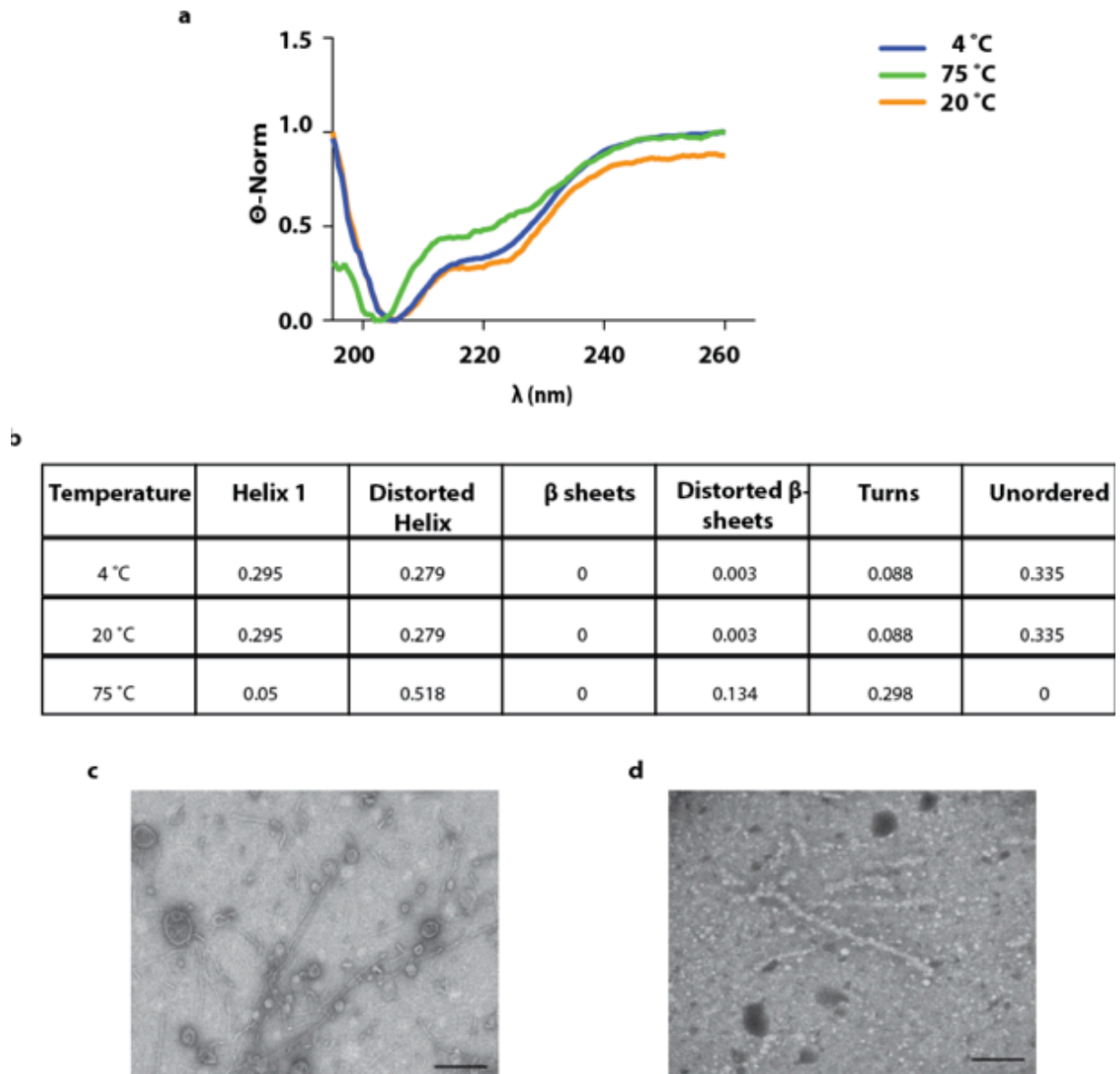


Figure 3.3. Hrp1 is predominantly helical

a) Determination of Hrp1 full-length secondary structure using CD. The conformational change was assessed at various temperatures. b) Quantification of secondary structures obtained from CD spectra (3a) using ContinLL algorithm. c) Elucidation of Hrp1 morphology using TEM. d) Elucidation of PrD domain using TEM. Scale bar 100 μm

3.3 Phosphate depletion has no effect on P-body formation

As determined above, Hrp1 undergoes phase separation and forms droplets exclusively under polyanionic conditions, such as, in the presence of polyacrylic acid. This finding supports the idea that the negatively charged polymer used in the screening might mimic the polyanionic nature of biopolymers existing in the cell namely DNA, RNA. Recently, the effect of RNA on LAF-1 protein droplets, which is a component of P-granules in *C. elegans*, was reported³⁰. This study demonstrated that RNA fluidizes the droplet using a microrheology approach³⁰. However, other polyanionic biopolymers have not been tested. We chose to examine the role of PolyP in P-body formation, because these cellular structures have been shown to undergo phase separation. First, we depleted inorganic phosphate from the growth medium of BY4741 yeast cells for six hours and induced P-body formation through glucose starvation. In the presence of glucose, the majority of the cells had no P-bodies, irrespective of whether the growth medium was supplemented with phosphate or not (**Figure 3.4.a** and **b**). However, glucose starvation induced P-body formation to a similar extent in the presence or absence of phosphate (**Figure 3.4.a** and **b**). As shown in **Figure 3.4.a**, P-bodies were readily identified in the cytoplasm following glucose starvation. Specifically, in +P_i-Glucose conditions, as well as in -P_i-Glucose conditions, the average number of P-bodies per cell was 1.3 (**Figure 3.4.b**). Moreover, the distribution P-bodies per cell was similar in the presence of glucose plus or minus phosphate (**Figure 3.4.c**). Glucose starvation induced a leftward shift in the distribution of P-bodies per cell plus or minus phosphate, suggesting that glucose depletion, but not phosphate depletion, induces P-body formation in the BY4741 strain. Notably, in the presence of glucose, only 2% of the cells had 1 P-body, while in the absence of glucose, more than 70% of the cells had 1 P-body. To determine whether there is a statistically significant difference between the cell populations grown under glucose starvation conditions in the presence compared to the absence of phosphate, the Mann-Whitney U-test was performed. However, the test revealed no statistically significant difference ($p > 0.05$). Lastly, given that increasing the concentration of multivalent ions has been shown to trigger swelling of polymer colloids, we sought to determine whether phosphate depletion affects the P-body size^{91,98}. The radii of P-bodies induced by glucose starvation were similar, irrespective of the presence or absence of phosphate in the growth medium, and ranged between 110 nm

and 230 nm (with an average of approximately 130 nm). The data in **Figure 3.4.d** is shown for two independent glucose starvation experiments only, because, as mentioned above, P-bodies did not form in the presence of glucose. Comparison of P-body size by the Mann-Whitney U-test revealed no statistically significant difference between the +P_i-Glucose and -P_i-Glucose conditions ($P > 0.05$). Taken together, these results demonstrate that phosphate depletion from the growth medium for six hours has no effect on P-body formation or P-body size. One possible explanation is that the lack of effect observed above was due to incomplete depletion of inorganic phosphate.

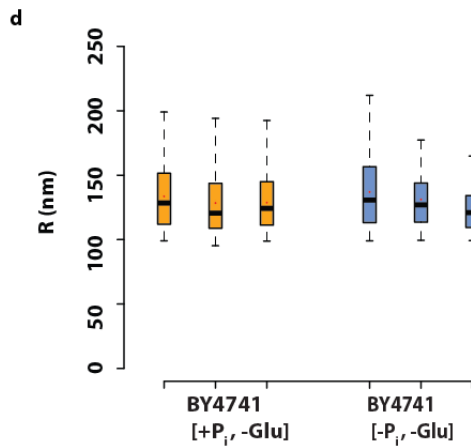
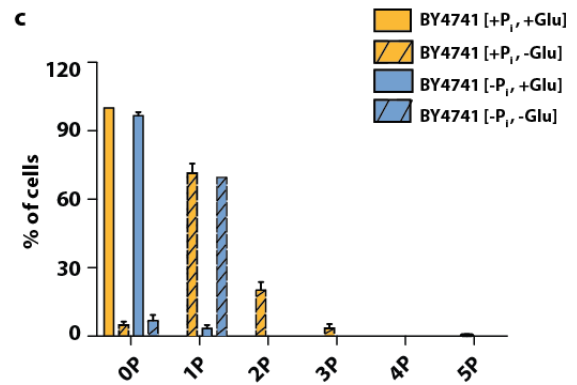
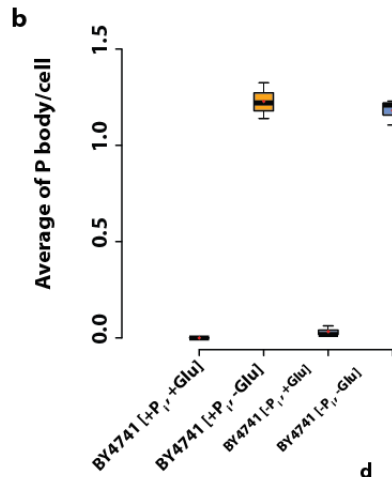
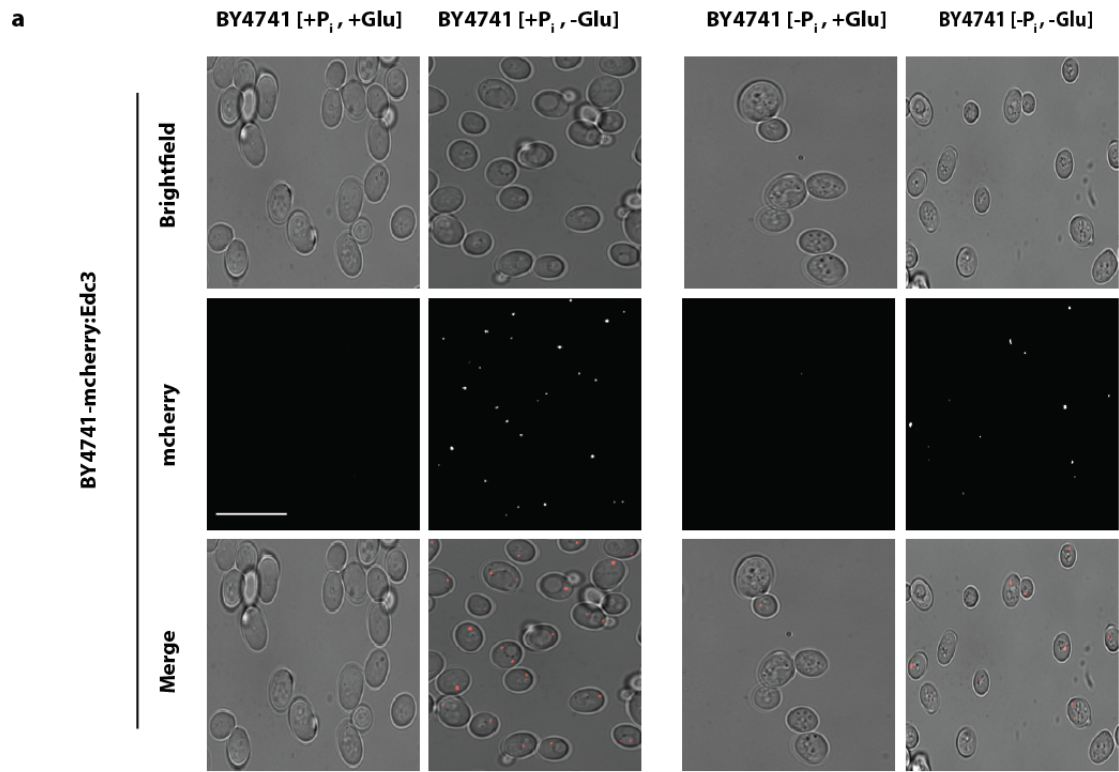


Figure 3.4. Phosphate depletion has no effect on P-body number and size

a) The wild type (By4741-mCherry-Edc3) was cultivated in phosphate-depleted or phosphate-sufficient media. P-bodies were induced under glucose starvation conditions and imaged using fluorescence microscopy. As a negative control, the wild type was incubated in a media containing glucose plus or minus phosphate. In the absence of glucose, P-bodies were observed both in phosphate-depleted and phosphate-sufficient media as compared to the negative control, where no P-bodies were observed. b) The average number of P-bodies per cell was determined in the presence and the absence of glucose in phosphate-depleted or phosphate-sufficient media. Under glucose starvation conditions, there was an increase in P-body numbers per cell both in phosphate-depleted and in phosphate-sufficient media as compared to the negative control. The average number of P-bodies per cell, in the absence of glucose, was identical regardless of whether the media lacks or contains phosphate. c) The distribution of P-bodies in a population of 100 cells was analyzed. Mann-Whitney U-test was used to analyze the significance of the population differences among the different conditions. Under glucose starvation, the wild type showed a wider distribution, while in the presence of glucose, the wild type showed a tighter distribution, regardless whether the media lacks or contains phosphate. d) Determination of the size of P-bodies under glucose-starvation conditions, in synthetic media containing or depleted of phosphate. The P-body size ranged from 110 nm to 230 nm. Scale bar 3 μm

3.4 Deletion of *vtc4* increases P-body numbers

To determine whether depletion of vacuolar PolyP have an effect on P-body formation *in vivo*, I generated a deletion of the *vtc4* gene by homologous recombination in the mCherry-Edc3 BY4741 strain. The mutant *vtc4Δ*-BY4741-mCherry-Edc3 and the wild type BY4741-mCherry-Edc3 yeast were grown to an OD₆₀₀ of 0.4 in complete synthetic media containing glucose. Subsequently, the cells were starved of glucose for 15 min and P-body formation was monitored using fluorescence microscopy. In the negative control, when the cells were grown in complete synthetic media, the wild type BY4741-mCherry-Edc3 yeast formed no P-bodies (**Figure 3.5.a** and b). By contrast, even in the presence of glucose, the *vtc4Δ*-BY4741-mCherry-Edc3 yeast exhibited on average 1 P-body per cell, suggesting that depletion of vacuolar PolyP induce cellular stress that leads to P-body formation. A comparison of the basal number of P-bodies per cell in the wild type and the *vtc4Δ* mutant strains, grown in the presence of glucose, showed a statistically significant difference by the student t-test ($p < 0.05$). Interestingly, glucose starvation further induced P-body formation both in the wild type BY4741-mCherry-Edc3 and in the mutant *vtc4Δ*-BY4741-mCherry-Edc3 strains to a similar extent, averaging approximately 2.3 and 3 P-bodies per cell, respectively (**Figure 3.5.b**).

Moreover, these differences between the wild type BY4741-mCherry-Edc3 and the mutant *vtc4Δ*-BY4741-mCherry-Edc3 strains were apparent in the distribution profiles of P-body numbers per cell when the strains were grown in the presence or absence of glucose (**Figure 3.5.c**). As noted in the previous section, glucose starvation (-Glucose) induced a shift to the right in the distribution of P-bodies per cell in the wild type BY4741-mCherry-Edc3 strain, compared to the +Glucose control, indicating an increase in P-body formation. Notably, in the presence of glucose, 92% of the cells had no P-bodies and only 4% of the cells had 1 P-body, while in the absence of glucose, approximately 40% of the cells had 1 P-body (Figure c). By contrast, in the presence of glucose, 42% of the mutant *vtc4Δ*-BY4741-mCherry-Edc3 cells had 1 P-body. Glucose starvation further induced P-body formation in the *vtc4Δ* mutant strain, with 87% of the cells exhibiting more than 1 P-body per cell (**Figure 3.5.c**). To determine whether there is a statistically significant difference between the wild type and the

vtc4Δ mutant cell populations grown in the presence or absence of glucose, the Mann-Whitney U-test was performed and a p-value < 0.05 was obtained.

Lastly, I sought to determine whether PolyP depletion affects P-body size, considering, as noted before, that polymer colloids have been shown to swell in the presence of increasing concentrations of multivalent ions^{91,98}. As shown in the box plots in **Figure 3.5.d**, the average radius of P-bodies (139 nm) found in *vtc4Δ* mutant cells grown in the absence of glucose was slightly greater than the average radius of P-bodies (100 nm) formed when the strain was grown in the presence of glucose. A p-value of 0.0014 was obtained for this comparison by a t-test, indicating statistical significance. Interestingly, the size of P-bodies formed in the absence of glucose in the wild type and in the *vtc4Δ* mutant were similar, ranging from approximately 110 nm to 230 nm (**Figure 3.5.d**). No statistical significance was obtained for this comparison ($P > 0.05$). Taken together, these data suggest that PolyP depletion induces cellular stress and P-body formation.

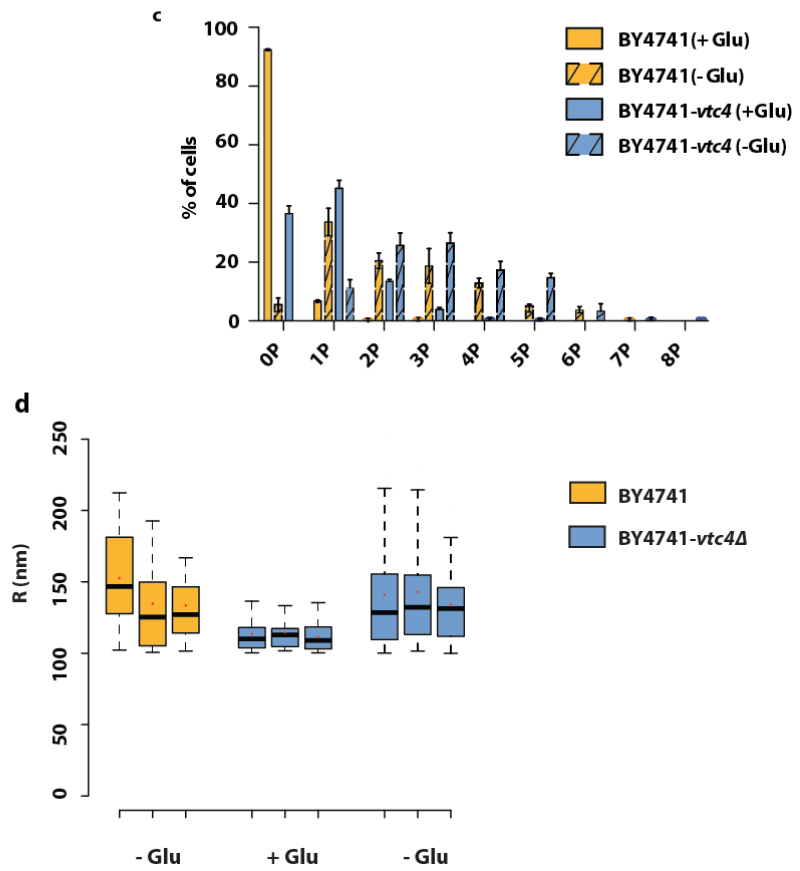
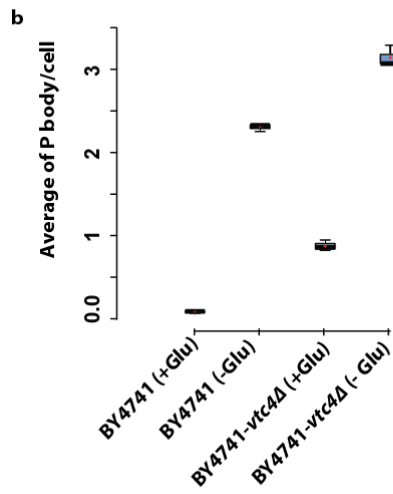
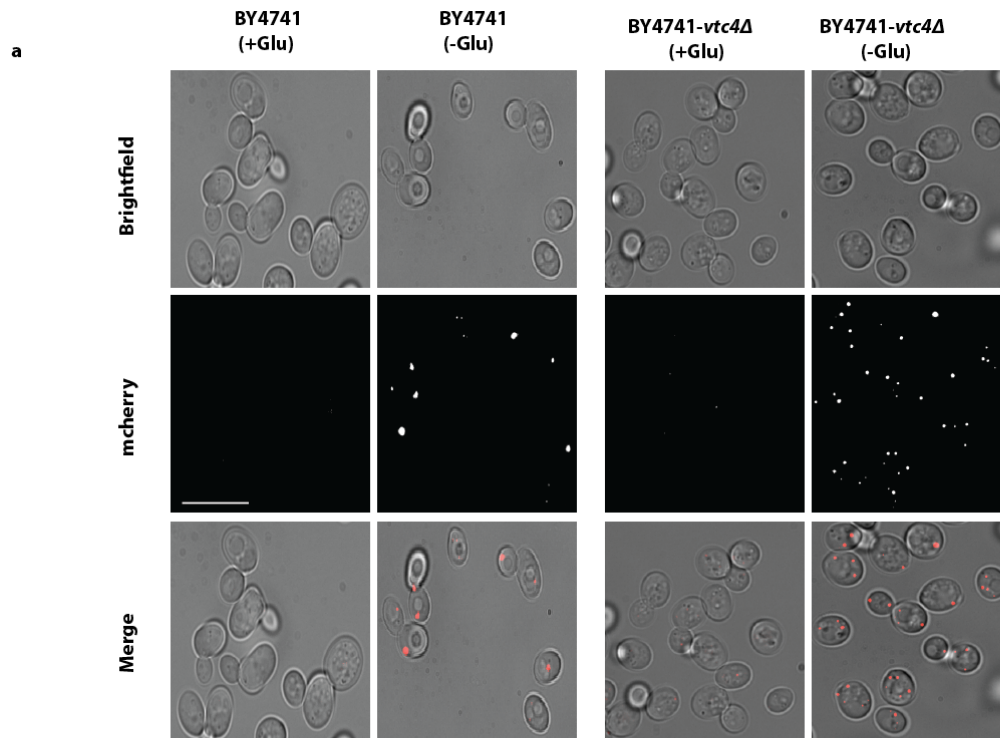


Figure 3.5. Deletion of *vtc4* gene leads to an increase in the number of P-bodies per cell

a-b) Removing glucose (-Glu) from the medium led to a significant increase in the average number of P-bodies both in the wild type and in the mutant strains, as compared to the negative controls. In the presence of glucose (+Glu), both the wild type and the $\Delta vtc4$ mutant strains displayed an average number of 0.08 and 1 P-body per cell, respectively, which was elevated to 2.3 and 3 P-bodies per cell under stress conditions, respectively. The wild type displayed an increase of thirty fold, while the $\Delta vtc4$ mutants exhibited an increase of 3 fold. c) The distribution of P-bodies in a population of 100 cells of BY4741 (WT) cells and BY4741:*vtc4* mutant cells was analyzed in the presence or absence of glucose (-Glu). In the absence of glucose, both the wild type and the $\Delta vtc4$ mutant strain displayed a wider P-body distribution as compared to the negative controls. P-body number per cell ranged from 1 to 8 P-bodies. By contrast, in the presence of glucose a tighter distribution was obtained. Specifically, the majority of the wild type population (~ 99%) exhibited 0 P-bodies per cell, while the distribution of P-bodies in the $\Delta vtc4$ mutant ranged from 0 to 3 P-bodies per cell. Approximately 80 % of the $\Delta vtc4$ mutant cells are equally distributed between 0 and 1 P-bodies per cell and the remaining 20 % are distributed between 2 and 3-P-bodies per cell d) A Box plot was generated to show the distribution of P-body radii in the wild type and in the $\Delta vtc4$ mutant strains under stress or non- stress conditions. The $\Delta vtc4$ mutant had an average P-body radius of 100 nm and 139 nm in the presence or absence of glucose, respectively ($p < 0.05$), indicating potentially different populations of P-bodies. By contrast, there was no significant difference in the average P-body size between the wild type and the $\Delta vtc4$ mutant strains in the absence of glucose ($P > 0.05$). Scale bar 3 μm

3.5 The PolyP does not associate with the P-body core component

Edc3

Polyphosphate (PolyP) are highly abundant in yeast and is found primarily in the vacuole and in the cytoplasm. As noted in the introduction, several studies have revealed a crucial role for negatively charged polymers, such as RNA, in the formation of liquid droplets³⁰. In addition, a recent study demonstrated that the nucleic acid mimic, Poly (ADP Ribose), triggers liquid-liquid phase separation of the intrinsically disordered proteins⁹⁹. Combined with my own findings that deletion of the gene involved in vacuolar PolyP synthesis, *vtc4Δ*, induces P-body formation, I sought, to examine whether PolyP co-localizes with P-bodies directly or whether it exerts an indirect effect, by regulating the cytoplasmic pH, for instance, since P-body droplets have been shown to be sensitive to changes in temperature²⁵, pH¹⁰⁰, and ionic strength³⁰.

To study the above, I first acquired the fluorescence absorbance spectrum of PolyP using DAPI counterstaining^{73,95}. Wild type BY4741 and mutant *vtc4Δ*-BY4741 cells were incubated at different OD₆₀₀ with DAPI for 30 minutes. DAPI was excited at a wavelength of 350 nm and the fluorescence emission was acquired between 400 and 650 nm. As illustrated in **Figure 3.6.b**, glucose starvation induced the formation of P-bodies, identified as m-Cherry labeled foci, which did not co-localize with DAPI-stained PolyP either in the wild type or in the *vtc4Δ* mutant yeast. In the wild type strain and in glucose-starved condition, it was not possible to discern between the fluorescence emitted from the mitochondrial network and that of the PolyP. The induced P-bodies in the wild type strain were found adjacent to the mitochondrial network. In contrast, the mutant lacked the mitochondrial DNA network and P-bodies were induced both in the presence and in the absence of glucose as previously reported. Consistent with a previous report, P-bodies marked by fluorescent tagging of the core component Edc3, were sometimes found adjacent to the mitochondrial network.

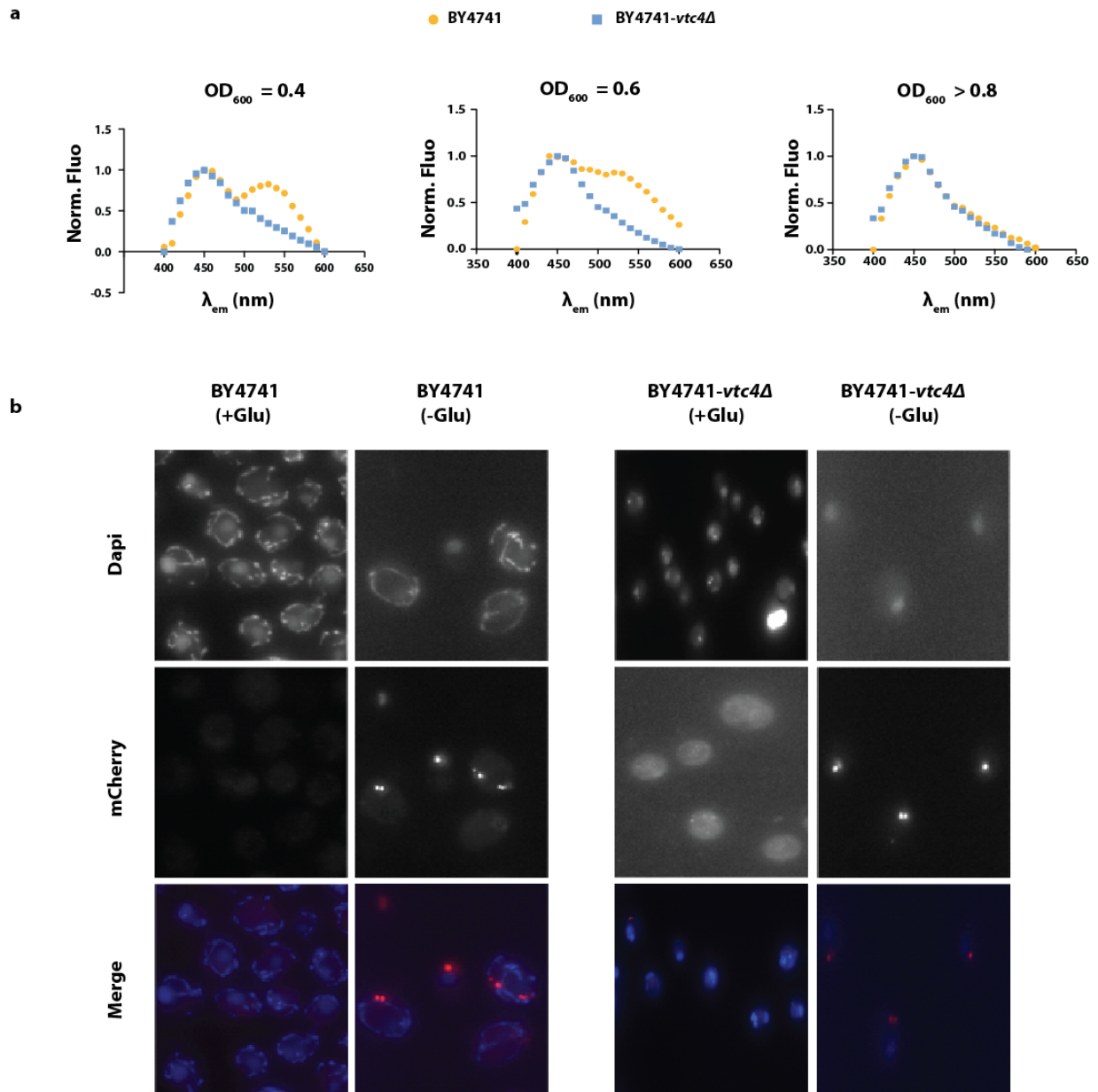


Figure 3.6. PolyP does not associate with P-bodies

a) Determination of PolyP absorption at different OD_{600} (0,4-0,6 and > 0,8) using the fluorimeter. The wild type and the $\Delta vt c 4$ mutant strains were excited at wavelength of 350 nm and the emission spectra were acquired over a range of 400 to 650 nm. b) Co-localization of the multivalent salt PolyP and P-bodies using the core component Edc3 as a marker

4 Discussion

A subset of specific proteins in the cell containing LCSs are able to self-assemble and form membrane-less organelles such as P-body. LCSs within these bodies undergo multiple weak interactions and form liquid state, the droplet; via liquid-liquid phase separation and misregulation of these membrane-less organelles could be pathological. Our goal in this study was on one hand, to investigate the physical state of the prion-like protein Hrp1 that could possibly form under certain conditions and on the other hand to decipher the role of PolyP in modulating the RNP-granule, P-body.

In this study, we demonstrated that the prion-like protein Hrp1, which contains the low complexity domain PolyQ/N undergoes phase separation and forms droplets *in vitro* in the presence of negatively charged polyelectrolytes. In contrast, the PolyQ/N domain and the RRM of Hrp1 form precipitates under the same conditions, suggesting that both domains are necessary for droplets formation. These findings are consistent with other studies suggesting that negatively charged polyelectrolytes or multivalent ions tune the electrostatic interactions between proteins and drive the phase separation of the protein in solution⁹³. The negatively charged polyelectrolyte under which droplets of Hrp1 formed mimics negatively charged biopolymers in the cell, including RNA, DNA and PolyP. Several studies demonstrated that proteins containing low complexity sequences undergo liquid-liquid phase separation *via* multiple promiscuous weak interactions between the mRNA and LCSs and homo/heterotypic interactions among LCS²¹. In addition, there is increasing appreciation that negatively charged RNA molecules are the driving forces for the formation of droplet assemblies in the cell^{21,22,30,33,96}. Zhang *et al.* (2015) demonstrated that the RNA binding protein whi3 in *Ashbya gossypii* forms droplets in the presence of RNA. Whi3 contains an expanded stretch of PolyQ and binds with varying affinity to two different RNAs that have different lengths, CLN3 (a G1 cyclin) and BNI1 (a formin encoding mRNA)¹⁰¹. Both mRNAs have 5 binding sites for whi3 protein. However, BNI1 mRNA is 4 times longer than CLN3 and its binding sites are distributed along the protein sequence, while Whi3 binding CLN3 mRNA is mainly at the 5' end of this transcripts¹⁰¹. The two distinct negatively charged mRNAs were able to modulate differently the biophysical properties of the Whi3 droplets, by decreasing fusion, by decreasing the exchange rate between the droplet and the bulk solution or by increasing the viscosity of the droplet²⁹. Surprisingly, these observations contradict the study achieved by Elbaum *et al.* (2015), where the authors observed that the non-specific polyU50 RNA fluidizes

the droplet forming by the P-granule disordered protein LAF-1. In the presence of RNA, the viscosity of LAF-1 protein droplets decreases. In addition, it is noteworthy to shed light on the specificity of RNAs toward their targets and their role in triggering phase transitions. For instance, non-specific mRNA does not trigger the phase separation of Whi3 protein, but it induces the phase separation of the promiscuous mRNA binding proteins, FUS, TDP43 and hnRNPA1^{32,43}. This suggests that the physical and chemical identity of negatively charged biopolymers, such as RNA, dictate not only the biophysical feature of the droplets but also induce the condensation or the dissolution of droplets in the cell.

The assembly of membrane-less compartments was thought at first to be driven by the oligomerization of low complexity domains. Mcknight *et al.* (2012) showed that the Low complexity domain of the FUS protein forms hydrogels under non-physiological conditions that have different properties than these of the droplets formed under physiological conditions. The low complexity sequence of FUS proteins contains a tyrosine that is flanked by either glycine or serine, and forms elongated fibrils. In this study, I showed that the LCS PolyQ/N of Hrp1, forms a gel-like material. However, the full-length protein was necessary to form droplets. This finding suggests that the LCS of Hrp1 protein favours intermolecular interactions over intramolecular interactions between the LCS and the solvent. We speculate that the LCS chains have higher affinity for each other (chain-chain) than for the solvent (chain-solvent), leading to aggregation and oligomerization, resulting in the formation of a gel-like material. Furthermore, this gel-like material may be driven by weak interactions between the Hrp1-LCSs, which are disrupted by an increase in temperature (data not shown). These results are in agreement with several studies^{3,33,102} and simultaneously are contradictory to many others³³. For instance, recent studies showed that the LCSs alone or in combination with RRM are able to undergo phase separation and form droplets. Specifically, Lin *et al.* (2015) investigated various LCSs derived from different proteins involved in distinct biological systems, including yeast and human RNP granules. The former involves Lsm4, eIF4GII and pub1 proteins components, and the latter includes FUS and hnRNPA1 proteins. Lsm4-LCS was shown to undergo phase separation and to form a stable but not well-defined microstructure, while the other proteins were shown to form droplets of different sizes and shapes. However, the Lsm4-LCS fused to Polypyrimidine Tract Binding Protein (PTB) forms

Lsm4 droplets in the presence of RNA. Moreover, it was suggested that liquid-liquid phase separation is driven by an orchestrated interactions of long-range interactions between charged motifs and short-range interactions of dipole-dipole and π - π stacking interaction as in the case of LAF1, DDx4 and hnRNPA1-LCSs^{25,30,31}. In addition, there is growing evidence that the liquid state, the droplet, is an intermediate for the solid-like state, which has been associated with different pathologies^{3,33-35,46,103}. The solid-like state assembles over time and is considered as an aging event that evolves through conformational changes that leads to fibrous state. For instance, the ALS-proteins FUS and hnRNPA1 exists in liquid state, which mature over time and form solid-like state. Ultimately, These findings suggest that the composition (the primary sequence) of LCSs that are embellished with charged pattern dictate the morphologies and the state of the assembled aggregates that leads to either droplets or fibrils formation.

The prion-like proteins containing LCSs are intrinsically disordered and can adopt various orientations resulting in several conformations through binding with their partners. The composition of the droplet and the various conformational orientations rule its organization and its shape. The collective behaviour of these heterogeneous matters within the droplet is still unclear. Specifically, it is not yet clear whether polymerized LCSs are embedded within the droplet or whether the RRM bound to mRNA is exposed to the surface (or vice versa). Therefore, attempts have been made to investigate the secondary structures that these proteins undergo and consequently understanding the organization of the Prion-like proteins embedded within droplets. In this study, the Hrp1 was revealed to be predominantly an alpha helical structure, while it was not possible to investigate the secondary structure of Hrp1-LCS-polyQ/N due to precipitation in the solution. Hrp1-LCS becomes opalescent, hindering CD analysis. However, it was suggested by CD analysis that PolyQ/N-LCSs derived from different proteins such as Htt (Huntingtin) and Ure2 have coiled coil domains through which the proteins can oligomerize. While, it was not possible to compare the secondary structure of the Hrp1 full-length protein and its LCS *via* CD analysis, we did elucidate the morphology of Hrp1 full-length protein and that of the LCS-PolyQ/N by TEM. Specifically, we showed that the LCS has an elongated morphology, whereas the full-length protein has both spherical and elongated conformation. We speculate that spherical morphology obtained

for Hrp1 full-length protein corresponds to the shape of droplets and the elongated morphologies are protein aggregations or contaminants. This finding is in agreement with the study made by Rosen *et al.* (2013), where it was shown that multiple weak interactions are the driving force for droplet formation, adopting spherical or ring conformation using TEM. By contrast, the LCS-PolyQ/N of Hrp1 is aggregation prone and forms filamentous conformation, which is consistent with Mcknight *et al.* (2012) study. This study showed that the LCS of FUS undergoes phase transition and forms hydrogel that has a filamentous conformation.

Ultimately, using the CD and TEM analysis were not sufficient to shed light on the organization of prion-like proteins within the droplet. In addition, the precipitation of Hrp1-LCS during CD analysis prevented us to further study the contribution of the critical amino acids *via* site directed mutagenesis that leads to liquid-state and consequently to compare Hrp1 full-length and Hrp1-LCS. However, Fromm *et al.* (2014) were able to decipher the intermolecular interactions that trigger liquid-liquid phase separation of the heterogeneous liquid body, the P-body. This study mapped *via* NMR the intermolecular interactions undergoing by the decapping enzyme Dcp2 and its activator Dcp1 as well as the scaffolding proteins such as Edc3 and Pdc1. They suggested that phase separation is triggered through intermolecular interactions between Edc3-LCS domain and 10 helical Leucine-rich motifs in Dcp2 and Pdc1 and blocking these interactions prevent phase separation.

Recent studies have shown that RNA triggers the assembly of phase-separated droplets. Interestingly, the negatively charged polyelectrolyte that induces Hrp1 droplets formation mimics both RNA and the highly abundant PolyP in *Saccharomyces cerevisiae*. PolyP regulate the cytosolic pH by sequestering amines in the vacuole. Considering a recent study demonstrating that acidification of the cytosol triggers the transition of the cytoplasm from a fluid state to a more solid-like state and consequently influences the organization of the macromolecule in the cytoplasm¹⁰⁴. We hypothesized that PolyP play a role in the assembly of the membrane-less organelles, such as P bodies.

We first investigated the effect of PolyP on P-body formation by disrupting the phosphate homeostasis in yeast through starvation for 6 hours, and found that this treatment had no influence either on P-body number or size. This was surprising given that most of the P-body core and scaffold components (Edc3, Lsm4, Pat1p, Dcp2 and Dcp1) are

phosphorylated^{105,106}. Moreover, previous studies have reported post-translational modifications such as phosphorylation among many parameters that influence droplet condensation and dissolution. These modifications are shown to enhance or diminish the net charge of intrinsically disordered protein above or below a critical threshold.

For instance, phosphorylation of the P-granule components MEG1 and MEG3 (maternal-effect germline defective) was recently shown to trigger the disassembly of the granule, while dephosphorylation promotes its assembly²³. One possible explanation to reconcile our findings with those of Wang *et al.* 2014 is that starvation of yeast for 6 hours results in incomplete phosphate depletion and that the residual cytoplasmic phosphate masks any effect on P-body formation²³.

For this reason, we abolished PolyP synthesis through deletion of the *vtc4* gene. We found that the mutant (BY4741-mcherry-Edc3- Δ *vtc4*) compared to the wild type yeast strain (BY4741-mcherry-Edc3) have higher number of P-bodies per cell under glucose starvation condition used to induce P-body formation and in the presence of glucose. This may be due to the fact that deletion of *vtc4* gene increases cellular stress overall. Interestingly, in the presence of glucose, P-body size was smaller than in the absence of glucose in the mutant strain. This suggests that different P-body populations are formed under different conditions. Furthermore, it is possible that different proteins and RNA are recruited to the P-body, allowing these bodies to grow under certain conditions to allow the cell to adjust to the environmental changes. Parker and co-workers shed light on the organization of the P-bodies⁵⁴. They suggested that the scaffold of the P-body recruits various proteins clients depending on the valency (free binding sites) of the scaffold. To validate our hypothesis concerning the formation of different population under certain condition, several experiments could be performed including ribosomal profiling and RNA-seq using the wild type strain and the Δ *vtc4* mutant grown in the presence and the absence of glucose. In addition, it would be important to determine whether P-bodies visualized using fluorescence microscopy are functional P-bodies undergoing dynamic structural changes. To discern between functional and non-functional P-bodies an RNA, known to localize to and be processed in P-bodies could be tagged and co-localized with mCherry labeled Edc3, a core component of P-body.

To further validate that PolyP do not associate with P-bodies, I performed a co-localization experiment between P-body core component Edc3 and PolyP. The former was labeled with mCherry, while the latter was stained with Dapi. PolyP were visualized using YFP filter. However, It was not possible to discern between the Dapi signal emitted from the mitochondrial network and the signal emitted from PolyP in the wild type strain. However, in glucose containing media, Ryazanova *et al.* (2011) were able to detect PolyP in the cytoplasm and in the mitochondria using Dapi to stain the cell and laser scanning microscopy to observe PolyP.

Ultimately, it is noteworthy, that in mammalian cells P-bodies interact physically with mitochondrial network for about 3 s and disruption of mitochondrial network did not affect P-bodies formation¹⁰⁷. In our study, in order to perform the co-localization experiment between PolyP and P-bodies, spectral imaging had to be carrying out to distinguish between the highly overlapping emission spectra of Dapi-mitochondria and Dapi-PolyP.

5 Conclusion and Perspectives

I demonstrated in this study that the mRNA binding protein Hrp1 full-length protein forms droplets in the presence of negatively charged polymer polyacrylic acid sodium salt. In contrast to the full-length protein, the N-terminal intrinsically disordered region of Hrp1 containing the Low complexity domain forms a gel-like material that is sensitive to temperature. Based on this initial study, we hypothesized that the negatively charged polyelectrolyte mimics polyphosphate (PolyP) in the cell. Depletion of phosphate from the media did not affect the condensation or the dissolution of P-bodies. Therefore, *vtc4* gene synthesizing PolyP was deleted using BY4741-mCherry-Edc3 as a background. Deletion of *vtc4* gene did not display any effect on P-body condensation or dissolution; instead an increase in the average number of P-body in the $\Delta vt c 4$ mutant strain resulted regardless whether it is under stress or not.

I think in this field the most challenging question that has emerged is why specific proteins containing LCSs undergo phase transition in the cell and why the liquid state is necessary to convey information or signal between compartments in the cell. In addition, what is the interplay between the LCSs and the RRM in a heterogeneous system such as P-body that promotes phase transition to a liquid-like state or solid-like state? And which components are essential to promote phase separation

under various stress condition? Determining the collective behaviour of these proteins enable us to decipher the universal physical phenomena behind their assembly, allowing the understanding of many biological processes.

To answer partially these questions, I began a pilot of experiments to study the assembly of P-bodies/droplets first *in vitro* using different proteins such as Ccr4, Pat1P, Dhh1, Edc3, Lsm4 and Pop2. These proteins are components of the core and the shell of P-bodies. I first chose the highly abundant P-body protein Dhh1. Dhh1 is an mRNA binding protein that contains two RRM and an intrinsically disordered region at the N and C-termini. 10 μ M of purified Dhh1 protein were subjected to different NaCl concentrations ranging from 25 mM to 500 mM and we found that Dhh1 droplets formed at concentrations of 100 mM and 200 mM NaCl (**Fig. S.7.4**).

To determine the interplay between LCSs and the necessary components that promote phase separation resulting in droplet formation, we could combine the previous mentioned proteins by respecting the stoichiometry under various condition *in vitro* and monitor for droplets formation using light microscopy. To further decipher the code embedded in the primary sequence of the P-body prion-like protein that mediate liquid-like or solid-like phase transition site directed mutagenesis could be performed. In particular, LCSs and proline residues within the LCSs of P-body that contribute to the flexibility of the multimodular domain could be mutated. For instance, the N-terminus of Dhh1 contains a stretch of PolyN, while the C-terminus contains a stretch of polyQ separated by two Prolines, It is intriguing to investigate whether these segments separately or in combination with other P-body components trigger phase transition. Ultimately, it would be interesting to study the physical properties of these assemblies using microrheology approach and how these properties are related to the function of P-body.

6 References

1. Malinovska, L., Kroschwald, S. & Alberti, S. Protein disorder, prion propensities, and self-organizing macromolecular collectives. *Biochim. Biophys. Acta* **1834**, 918–31 (2013).
2. Lee, C. F., Brangwynne, C. P., Gharakhani, J., Hyman, A. a. & Jülicher, F. Spatial Organization of the Cell Cytoplasm by Position-Dependent Phase Separation. *Phys. Rev. Lett.* **111**, 88101 (2013).
3. Kato, M. *et al.* Cell-free formation of RNA granules: low complexity sequence domains form dynamic fibers within hydrogels. *Cell* **149**, 753–67 (2012).
4. Newby, G. a & Lindquist, S. Blessings in disguise: biological benefits of prion-like mechanisms. *Trends Cell Biol.* **23**, 251–259 (2013).
5. Das, R. K., Ruff, K. M. & Pappu, R. V. Relating sequence encoded information to form and function of intrinsically disordered proteins. *Curr. Opin. Struct. Biol.* **32**, 102–112 (2015).
6. Das, R. K. & Pappu, R. V. Conformations of intrinsically disordered proteins are influenced by linear sequence distributions of oppositely charged residues. *Proc. Natl. Acad. Sci. U. S. A.* **110**, 13392–7 (2013).
7. Mao, A. H., Lyle, N. & Pappu, R. V. Describing sequence–ensemble relationships for intrinsically disordered proteins. *Biochem. J.* **449**, 307–318 (2013).
8. Toombs, J. a, McCarty, B. R. & Ross, E. D. Compositional determinants of prion formation in yeast. *Mol. Cell. Biol.* **30**, 319–32 (2010).
9. Updike, D. L., Hachey, S. J., Kreher, J. & Strome, S. P granules extend the nuclear pore complex environment in the *C. elegans* germ line. *J. Cell Biol.* **192**, 939–48 (2011).
10. Prusiner, S. B. Prions causing degenerative neurological diseases. *Annu. Rev. Med.* **38**, 381–398 (1987).
11. Alberti, S., Halfmann, R., King, O., Kapila, A. & Lindquist, S. A systematic survey identifies prions and illuminates sequence features of prionogenic proteins. *Cell* **137**, 146–158 (2009).
12. Shorter, J. & Lindquist, S. Prions as adaptive conduits of memory and inheritance. *Nat. Rev. Genet.* **6**, 435–450 (2005).
13. Williamson, T. E., Vitalis, A., Crick, S. L. & Pappu, R. V. Modulation of polyglutamine conformations and dimer formation by the N-terminus of huntingtin. *J. Mol. Biol.* **396**, 1295–309 (2010).
14. Halfmann, R. *et al.* Opposing effects of glutamine and asparagine govern prion formation by intrinsically disordered proteins. *Mol. Cell* **43**, 72–84 (2011).
15. Ader, C. *et al.* Amyloid-like interactions within nucleoporin FG hydrogels. *Proc. Natl. Acad. Sci. U. S. A.* **107**, 6281–5 (2010).

16. Petri, M., Frey, S., Menzel, A., Görlich, D. & Techert, S. Structural characterization of nanoscale meshworks within a nucleoporin FG hydrogel. *Biomacromolecules* **13**, 1882–9 (2012).
17. Brangwynne, C. P. Soft active aggregates: mechanics, dynamics and self-assembly of liquid-like intracellular protein bodies. *Soft Matter* **7**, 3052 (2011).
18. Brangwynne, C. P., Mitchison, T. J. & Hyman, A. a. Active liquid-like behavior of nucleoli determines their size and shape in *Xenopus laevis* oocytes. *Proc. Natl. Acad. Sci. U. S. A.* **108**, 4334–9 (2011).
19. Hyman, A. A. & Brangwynne, C. P. Beyond stereospecificity: liquids and mesoscale organization of cytoplasm. *Dev. Cell* **21**, 14–6 (2011).
20. Wippich, F. *et al.* Dual specificity kinase DYRK3 couples stress granule condensation/dissolution to mTORC1 signaling. *Cell* **152**, 791–805 (2013).
21. Li, P. *et al.* Phase transitions in the assembly of multivalent signalling proteins. *Nature* **483**, 336–40 (2012).
22. Zhang, H. *et al.* RNA Controls PolyQ Protein Phase Transitions. *Mol. Cell* **60**, 220–30 (2015).
23. Wang, J. T. *et al.* Regulation of RNA granule dynamics by phosphorylation of serine-rich, intrinsically-disordered proteins in *C. elegans*. *Elife* **3**, 1–23 (2014).
24. Aumiller, W. M. & Keating, C. D. Phosphorylation-mediated RNA/peptide complex coacervation as a model for intracellular liquid organelles. *Nat. Chem.* **8**, 129–137 (2015).
25. Nott, T. J. *et al.* Phase Transition of a Disordered Nuage Protein Generates Environmentally Responsive Membraneless Organelles. *Mol. Cell* **57**, 936–947 (2015).
26. Sokolova, E. *et al.* Enhanced transcription rates in membrane-free protocells formed by coacervation of cell lysate. *Proc. Natl. Acad. Sci. U. S. A.* **110**, 11692–7 (2013).
27. Pielak, G. J. A model of intracellular organization. *Proc. Natl. Acad. Sci. U. S. A.* **102**, 5901–2 (2005).
28. Johansen, D., Jeffries, C. M. J., Hammouda, B., Trehwella, J. & Goldenberg, D. P. Effects of macromolecular crowding on an intrinsically disordered protein characterized by small-angle neutron scattering with contrast matching. *Biophys. J.* **100**, 1120–1128 (2011).
29. Lin, Y. *et al.* Formation and Maturation of Phase-Separated Liquid Droplets by RNA-Binding Proteins Article Formation and Maturation of Phase-Separated Liquid Droplets by RNA-Binding Proteins. *Mol. Cell* **60**, 1–12 (2015).
30. Elbaum-garfinkle, S., Kim, Y., Szczepaniak, K. & Chen, C. C. The disordered P granule protein LAF-1 drives phase separation into droplets with tunable viscosity and dynamics. 1–6 (2015). doi:10.1073/pnas.1504822112
31. Brangwynne, C. P., Tompa, P. & Pappu, R. V. Polymer Physics of Intracellular Phase Transitions. **11**, 1–13 (2015).

32. Burke, K. A., Janke, A. M., Rhine, C. L. & Fawzi, N. L. Residue-by-Residue View of In Vitro FUS Granules that Bind the C-Terminal Domain of RNA Polymerase II. *Mol. Cell* **60**, 1–11 (2015).
33. Lin, Y. *et al.* Formation and Maturation of Phase-Separated Liquid Droplets by RNA-Binding Proteins Article Formation and Maturation of Phase-Separated Liquid Droplets by RNA-Binding Proteins. *Mol. Cell* **60**, 1–12 (2015).
34. Molliex, A. *et al.* Phase Separation by Low Complexity Domains Promotes Stress Granule Assembly and Drives Pathological Fibrillization Article Phase Separation by Low Complexity Domains Promotes Stress Granule Assembly and Drives Pathological Fibrillization. *Cell* **163**, 123–133 (2015).
35. Patel, A. *et al.* A Liquid-to-Solid Phase Transition of the ALS Protein FUS Accelerated by Disease Mutation. *Cell* **162**, (2015).
36. Kroschwald, S. *et al.* Promiscuous interactions and protein disaggregases determine the material state of stress-inducible RNP granules. *Elife* **4**, (2015).
37. Pérez-Cañadillas, J. M. Grabbing the message: structural basis of mRNA 3'UTR recognition by Hrp1. *EMBO J.* **25**, 3167–78 (2006).
38. Niño, C. a, Hérisant, L., Babour, A. & Dargemont, C. mRNA Nuclear Export in Yeast. *Chem. Rev.* (2013). doi:10.1021/cr400002g
39. Kessler, M. M. *et al.* Hrp1, a sequence-specific RNA-binding protein that shuttles between the nucleus and the cytoplasm, is required for mRNA 3'-end formation in yeast. *Genes Dev.* **11**, 2545–2556 (1997).
40. Valentini, S. R., Weiss, V. H. & Silver, P. A. Arginine methylation and binding of Hrp1p to the efficiency element for mRNA 3'-end formation. *RNA* **5**, 272–80 (1999).
41. Mitchell, S. F., Jain, S., She, M. & Parker, R. Global analysis of yeast mRNPs. *Nat. Struct. Mol. Biol.* **20**, 127–33 (2013).
42. Decker, C. J. & Parker, R. P-bodies and stress granules: possible roles in the control of translation and mRNA degradation. *Cold Spring Harb. Perspect. Biol.* **4**, 1–18 (2012).
43. Molliex, A. *et al.* Phase Separation by Low Complexity Domains Promotes Stress Granule Assembly and Drives Pathological Fibrillization. *Cell* **163**, 123–133 (2015).
44. Jain, S. *et al.* ATPase-Modulated Stress Granules Contain a Diverse Proteome and Substructure. *Cell* **164**, 487–498 (2016).
45. Dewey, C. M. *et al.* TDP-43 is directed to stress granules by sorbitol, a novel physiological osmotic and oxidative stressor. *Mol. Cell. Biol.* **31**, 1098–108 (2011).
46. Li, Y. R., King, O. D., Shorter, J. & Gitler, A. D. Stress granules as crucibles of ALS pathogenesis. *J. Cell Biol.* **201**, 361–372 (2013).
47. Parker, R. & Sheth, U. P Bodies and the Control of mRNA Translation and Degradation. *Mol. Cell* **25**, 635–646 (2007).
48. Collier, J. M., Tucker, M., Sheth, U., Valencia-Sanchez, M. a & Parker, R. The DEAD box helicase, Dhh1p, functions in mRNA decapping and interacts with both the

- decapping and deadenylase complexes. *RNA* **7**, 1717–1727 (2001).
49. Mok, J. *et al.* NIH Public Access. **3**, (2011).
 50. Reijns, M. A. M., Alexander, R. D., Spiller, M. P. & Beggs, J. D. A role for Q/N-rich aggregation-prone regions in P-body localization. *J. Cell Sci.* **121**, 2463–72 (2008).
 51. Teixeira, D., Sheth, U., Valencia-Sanchez, M. a, Brengues, M. & Parker, R. Processing bodies require RNA for assembly and contain nontranslating mRNAs. *RNA* **11**, 371–382 (2005).
 52. Ashe, M. P., Long, S. K. De & Sachs, A. B. Initiation in Yeast. **11**, 833–848 (2000).
 53. Fromm, S. a. *et al.* InVitro reconstitution of a cellular phase-transition process that involves the mRNA decapping machinery. *Angew. Chemie - Int. Ed.* **53**, 7354–7359 (2014).
 54. Banani, S. F. *et al.* Compositional Control of Phase-Separated Cellular Bodies. *Cell* 1–13 (2016). doi:10.1016/j.cell.2016.06.010
 55. Kulaev, I. S., Vagabov, V. M. & Kulakovskaya, T. V. *The Biochemistry of Inorganic Polyphosphates: Second Edition. The Biochemistry of Inorganic Polyphosphates: Second Edition* (2005). doi:10.1002/0470858192
 56. Meyer, A. Orientierende Untersuchungen überverbreitung, Morphologie, und chemie des volutins. *Bot. Zeit.* **62(1)**, 113–152 (1904).
 57. Kornberg, a. Inorganic polyphosphate: Toward making a forgotten polymer unforgettable. *J. Bacteriol.* **177**, 491–496 (1995).
 58. Kornberg, A., Rao, N. N. & Ault-Riché, D. INORGANIC POLYPHOSPHATE: A Molecule of Many Functions. *Annu. Rev. Biochem.* **68**, 89–125 (1999).
 59. Achbergerová, L. & Nahálka, J. Polyphosphate - an ancient energy source and active metabolic regulator. *Microb. Cell Fact.* **10**, 63 (2011).
 60. Wurst, H. & Kornberg, A. A soluble exopolyphosphatase of *Saccharomyces cerevisiae*. Purification and characterization. *J. Biol. Chem.* **269**, 10996–11001 (1994).
 61. Andreeva, N. A. & Okorokov, L. A. Purification and characterization of highly active and stable polyphosphatase from *Saccharomyces cerevisiae* cell envelope. *Yeast* **9**, 127–139 (1993).
 62. Dunn, T., Gable, K. & Beeler, T. Regulation of cellular Ca²⁺ by yeast vacuoles. *J. Biol. Chem.* **269**, 7273–7278 (1994).
 63. Pick, U. & Weiss, M. Polyphosphate Hydrolysis within Acidic Vacuoles in Response to Amine-Induced Alkaline Stress in the Halotolerant Alga *Dunaliella salina*. *Plant Physiol.* **97**, 1234–40 (1991).
 64. Offenbacher, S. & Kline, E. S. Evidence for polyphosphate in phosphorylated nonhistone nuclear proteins. *Arch. Biochem. Biophys.* **231**, 114–123 (1984).
 65. Nomura, K., Kato, J., Takiguchi, N., Ohtake, H. & Kuroda, A. Effects of inorganic polyphosphate on the proteolytic and DNA-binding activities of Lon in *Escherichia*

- coli. *J. Biol. Chem.* **279**, 34406–34410 (2004).
66. Gray, M. *et al.* Polyphosphate Is a Primordial Chaperone. *Mol. Cell* **53**, 689–699 (2014).
 67. Cremers, C. M. *et al.* Polyphosphate: A Conserved Modifier of Amyloidogenic Processes. *Mol. Cell* **63**, 1–13 (2016).
 68. Werner, T. P., Amrhein, N. & Freimoser, F. M. Specific localization of inorganic polyphosphate (poly P) in fungal cell walls by selective extraction and immunohistochemistry. *Fungal Genet. Biol.* **44**, 845–852 (2007).
 69. Gerasimaitė, R., Sharma, S., Desfougères, Y., Schmidt, A. & Mayer, A. Coupled synthesis and translocation restrains polyphosphate to acidocalcisome-like vacuoles and prevents its toxicity. *J. Cell Sci.* **127**, 5093–104 (2014).
 70. Lichko, L. P., Kulakovskaya, T. V, Kulakovskaya, E. V & Kulaev, I. S. Inactivation of PPX1 and PPN1 genes encoding exopolyphosphatases of *Saccharomyces cerevisiae* does not prevent utilization of polyphosphates as phosphate reserve. *Biochemistry. Biokhimiia* **73**, 985–989 (2008).
 71. Secco, D., Wang, C., Shou, H. & Whelan, J. Phosphate homeostasis in the yeast *Saccharomyces cerevisiae*, the key role of the SPX domain-containing proteins. *FEBS Lett.* **586**, 289–295 (2012).
 72. Shirahama, K., Yazaki, Y., Sakano, K., Wada, Y. & Ohsumi, Y. Vacuolar function in the phosphate homeostasis of the yeast *Saccharomyces cerevisiae*. *Plant Cell Physiol.* **37**, 1090–3 (1996).
 73. Ryazanova, L. The early stage of polyphosphate accumulation in *Saccharomyces cerevisiae*: comparative study by extraction and DAPI staining. *Adv. Biosci. Biotechnol.* **2**, 293–297 (2011).
 74. Indge, K. J. Polyphosphates of the yeast cell vacuole. *J. Gen. Microbiol.* **51**, 447–455 (1968).
 75. M. Dürr, K. Urech, Th. Boller, A. Wiemken, J. Schwencke, M. N. Sequestration of arginine by polyphosphosphate in vacuoles of yeast. *Arch. Microbiol.* **121**, 169–175
 76. Azevedo, C., Livermore, T. & Saiardi, A. Protein Polyphosphorylation of Lysine Residues by Inorganic Polyphosphate. *Mol. Cell* **58**, 71–82 (2015).
 77. Odom, a R., Stahlberg, a, Wentte, S. R. & York, J. D. A role for nuclear inositol 1,4,5-trisphosphate kinase in transcriptional control. *Science* **287**, 2026–2029 (2000).
 78. Burton, A., Azavedo, C., Riccio, a & Saiardi, a. Inositol pyrophosphates regulate JMJD2C-dependent histone demethylation. **110**, 1–6 (2010).
 79. Shen, X., Xiao, H., Ranallo, R., Wu, W.-H. & Wu, C. Modulation of ATP-dependent chromatin-remodeling complexes by inositol polyphosphates. *Science* **299**, 112–114 (2003).
 80. Shears, S. B. Inositol pyrophosphates: Why so many phosphates? *Adv. Biol. Regul.* **57**, 203–216 (2015).

81. Steger, D. J., Haswell, E. S., Miller, A. L., Wentz, S. R. & O'Shea, E. K. Regulation of chromatin remodeling by inositol polyphosphates. *Science* **299**, 114–116 (2003).
82. Bennett, M., Onnebo, S. M. N., Azevedo, C. & Saiardi, A. Inositol pyrophosphates: Metabolism and signaling. *Cell. Mol. Life Sci.* **63**, 552–564 (2006).
83. York, J. D., Odom, R., Murphy, R., Ives, E. B. & Wentz, S. R. A phospholipase C-dependent inositol polyphosphate kinase pathway required for efficient messenger RNA export. *Science* **285**, 96–100 (1999).
84. Saiardi, A., Sciambi, C., McCaffery, J. M., Wendland, B. & Snyder, S. H. Inositol pyrophosphates regulate endocytic trafficking. *Proc. Natl. Acad. Sci. U. S. A.* **99**, 14206–14211 (2002).
85. Azevedo, C., Burton, A., Bennett, M., Onnebo, S. M. N. & Saiardi, A. Synthesis of InsP7 by the Inositol Hexakisphosphate Kinase 1 (IP6K1). *Methods Mol. Biol.* **645**, 73–85 (2010).
86. Bhandari, R. *et al.* Protein pyrophosphorylation by inositol pyrophosphates is a posttranslational event. *Proc. Natl. Acad. Sci. U. S. A.* **104**, 15305–15310 (2007).
87. Livermore, T. M., Azevedo, C., Kolozsvari, B., Wilson, M. S. C. & Saiardi, A. Phosphate, inositol and polyphosphates. *Biochem. Soc. Trans.* **44**, 253–259 (2016).
88. Williams, S. P., Gillaspay, G. E. & Perera, I. Y. Biosynthesis and possible functions of inositol pyrophosphates in plants. *Front. Plant Sci.* **6**, 1–12 (2015).
89. Saiardi, A., Bhandari, R., Resnick, A. C., Snowman, A. M. & Snyder, S. H. Phosphorylation of proteins by inositol pyrophosphates. *Science* **306**, 2101–2105 (2004).
90. Brangwynne, C. P. *et al.* Germline P granules are liquid droplets that localize by controlled dissolution/condensation. *Science* **324**, 1729–32 (2009).
91. Saunders, B. Microgel particles as model colloids: theory, properties and applications. *Adv. Colloid Interface Sci.* **80**, 1–25 (1999).
92. Campus, N. & manu. Polyamines in Modulating Protein Aggregation. *J. proteins proteomics* **3**, 1–10 (2012).
93. Wong, G. C. L. & Pollack, L. Electrostatics of strongly charged biological polymers: ion-mediated interactions and self-organization in nucleic acids and proteins. *Annu. Rev. Phys. Chem.* **61**, 171–189 (2010).
94. Tang, J. X. & Janmey, P. A. The Polyelectrolyte Nature of F-actin and the Mechanism of Actin Bundle Formation. *J. Biol. Chem.* **271**, 8556–8563 (1996).
95. Kolozsvari, B., Parisi, F. & Saiardi, A. Inositol phosphates induce DAPI fluorescence shift. *Biochem. J.* **460**, 377–85 (2014).
96. Guo, L. & Shorter, J. It's Raining Liquids: RNA Tunes Viscoelasticity and Dynamics of Membraneless Organelles. *Mol. Cell* **60**, 189–192 (2015).
97. Sreerama, N. & Woody, R. W. in *Circular Dichroism: Principles and Applications* 601–620 (2000).

98. Lipowsky, R. *et al.* Droplets, bubbles, and vesicles at chemically structured surfaces. *J. Phys. Condens. Matter* **17**, S537–S558 (2005).
99. Altmeyer, M. *et al.* Liquid demixing of intrinsically disordered proteins is seeded by poly(ADP-ribose). *Nat. Commun.* **6**, 8088 (2015).
100. Iwaki, A. & Izawa, S. Acidic stress induces the formation of P-bodies, but not stress granules, with mild attenuation of bulk translation in *Saccharomyces cerevisiae*. *Biochem. J.* **446**, 225–33 (2012).
101. Zhang, H. *et al.* RNA Controls PolyQ Protein Phase Transitions. *Mol. Cell* **60**, 220–230 (2015).
102. Xiang, S. *et al.* The LC Domain of hnRNPA2 Adopts Similar Conformations in Hydrogel Polymers, Liquid-like Droplets, and Nuclei. *Cell* **163**, (2015).
103. Weber, S. C. & Brangwynne, C. P. Getting RNA and protein in phase. *Cell* **149**, 1188–91 (2012).
104. Munder, M. C. *et al.* A pH-driven transition of the cytoplasm from a fluid- to a solid-like state promotes entry into dormancy. *Elife* **5**, e09347 (2016).
105. Swaney, D. L. *et al.* Global analysis of phosphorylation and ubiquitylation cross-talk in protein degradation. *Nat. Methods* **10**, 676–82 (2013).
106. Albuquerque, C. P. *et al.* A multidimensional chromatography technology for in-depth phosphoproteome analysis. *Mol. Cell. Proteomics* **7**, 1389–1396 (2008).
107. Huang, L. *et al.* Mitochondria associate with P-bodies and modulate microRNA-mediated RNA interference. *J. Biol. Chem.* **286**, 24219–24220 (2011).

7 Appendix

7.1 Supplementary figures

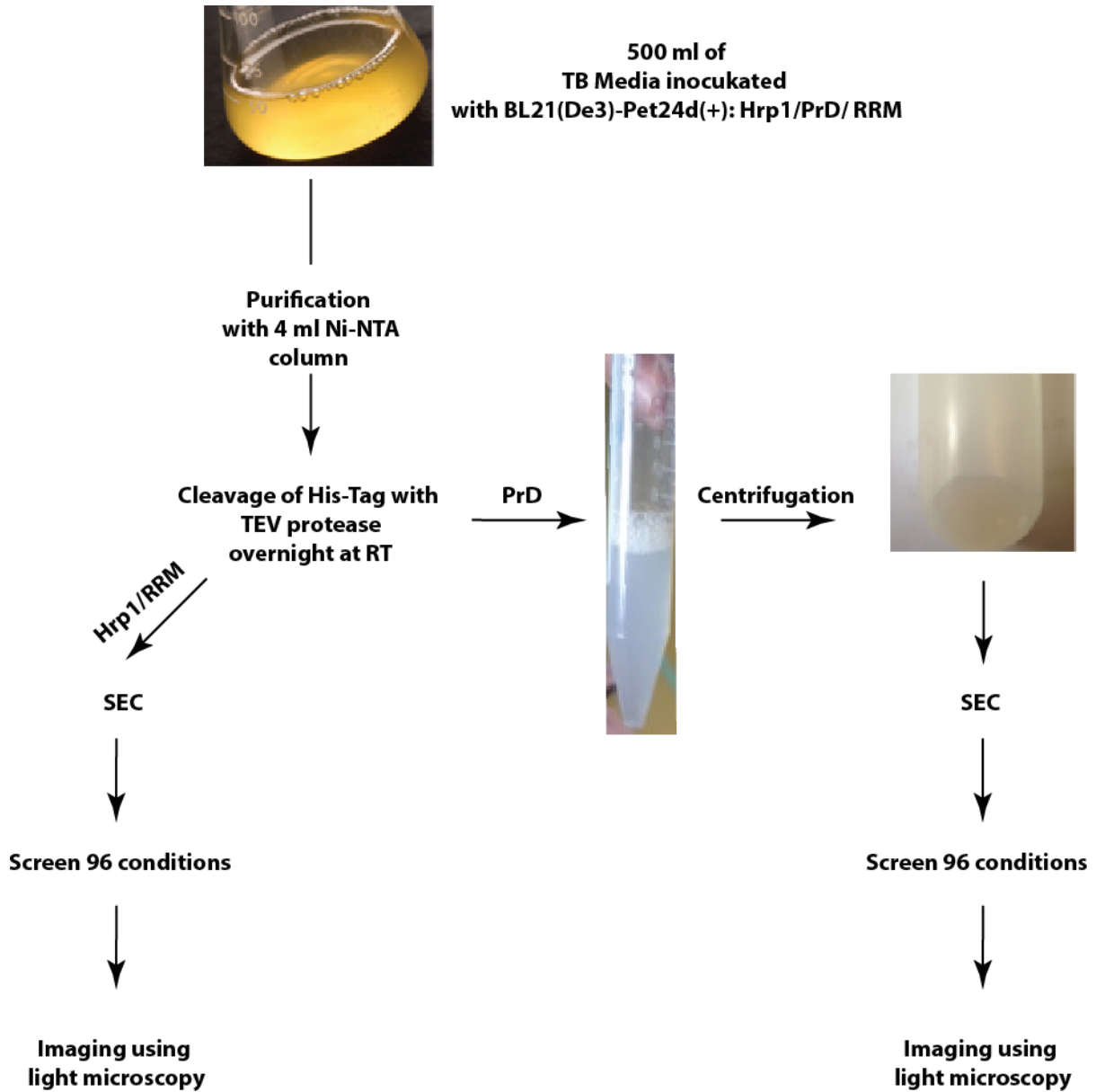


Fig.S 7.1 Scheme for Hrp1 purification and its variants

500 ml of TB Media was inoculated with BL21 (De3) harbouring the indicated constructs. Proteins expression was induced with 1 mM IPTG for 4 hours at 37 °C. The lysates were loaded on NI-NTA column. Subsequently, the tag was cleaved with Tev protease and the proteins were loaded onto size exclusion chromatography column for further purification. Hrp1 and the RRM proteins were subjected to 96 screening conditions. The PrD forms an opalescent solution during incubation at RT overnight. A gel-like material formed after centrifugation. The supernatant was removed, concentrated with an Amicon-ultra column, loaded onto a size exclusion chromatography and then subjected to 96 screening conditions

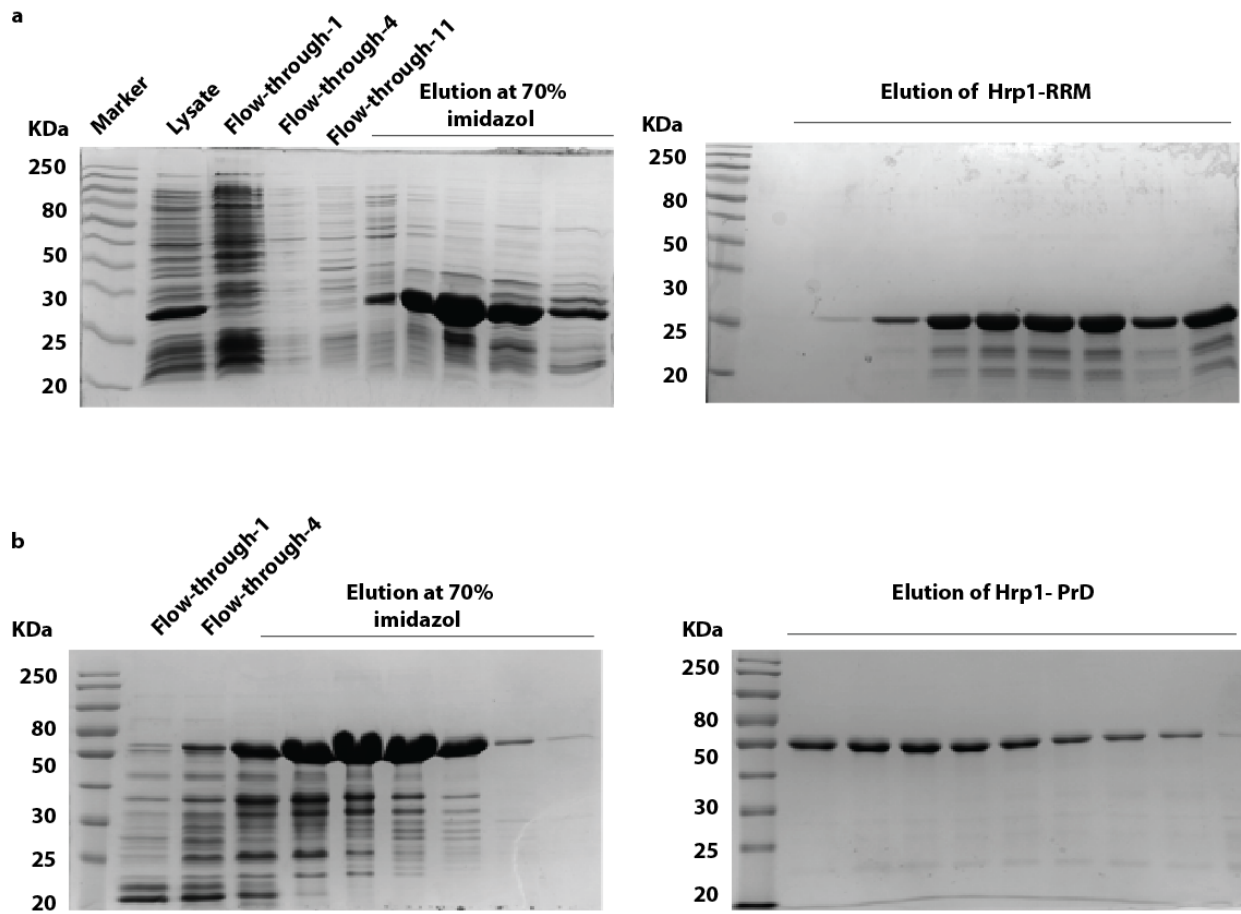


Fig.S 7.2.SDS-PAGE of RRM and PrD after affinity chromatography and Size exclusion chromatography

a-b) Similar to Hrp1, RRM and PrD were purified by loading the lysate on NI-NTA column and size exclusion chromatography. The variants were eluted in stepwise gradient of imidazole. Consequently, they were eluted at 70% of imidazole. The His-tev tag was also cleaved with Tev protease enzyme (data not shown). The RRM and PrD were migrated at a MW higher than expected in panel a and b, respectively

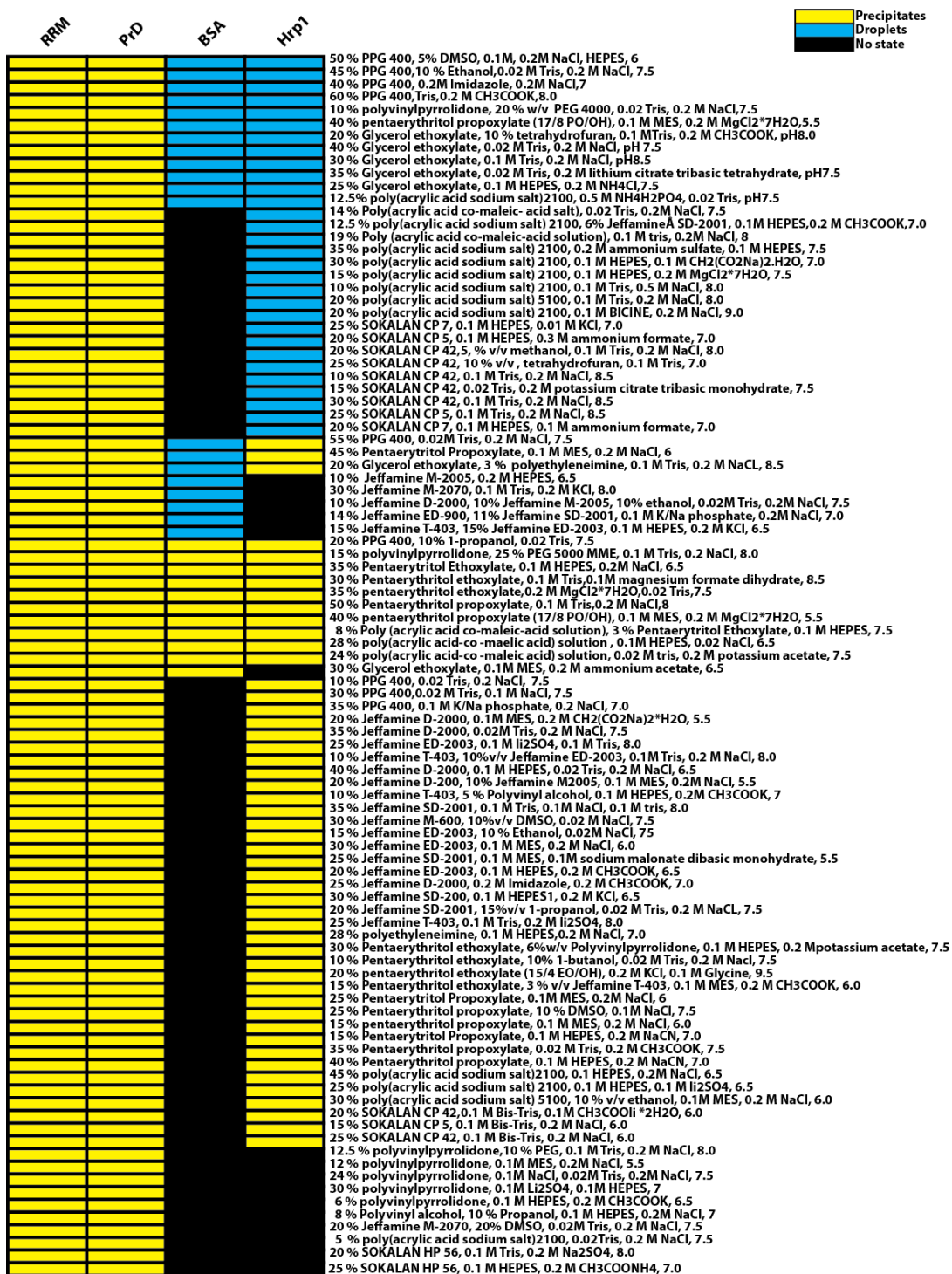


Fig.S 7.3. Screening for droplet formation

Hrp1 and RRM form precipitates, whereas Hrp1 forms droplets solely under poly (acrylic acid sodium) salt and its derivative. The negative control BSA under these conditions forms nothing, whereas under positively charged condition droplets were formed

7.2 Dhh1 protein forms droplets under physiological salt concentration

To study the assembly of the P-bodies/droplets first *in vitro* using different proteins such as Ccr4, Pat1P, Dhh1, Edc3, Lsm4 and Pop2. Toward that goal, I amplified these genes via PCR and cloned them into Pet24d(+) containing a His-Tev tag. In this system, the proteins were well expressed in BLR(DE3) upon induction with 1mM IPTG overnight in Terrific Broth (TB) media. Unfortunately, the proteins were not soluble. Therefore I tried different solubilization conditions, such as Urea, RIPA buffer, 1% SDS, Tris/HCl and finally Arginine mono-hydrochloride. I found that the recombinant proteins were soluble in non-denaturing conditions; namely in 1M Arginine mono-hydrochloride. I solubilized the recombinant Dhh1 protein in 1M Arginine mono-hydrochloride, subjected it to Sephadex G25 to remove the 1M Arginine mono-hydrochloride, and further purified Dhh1 using NI-NTA and Ion-exchange chromatography.

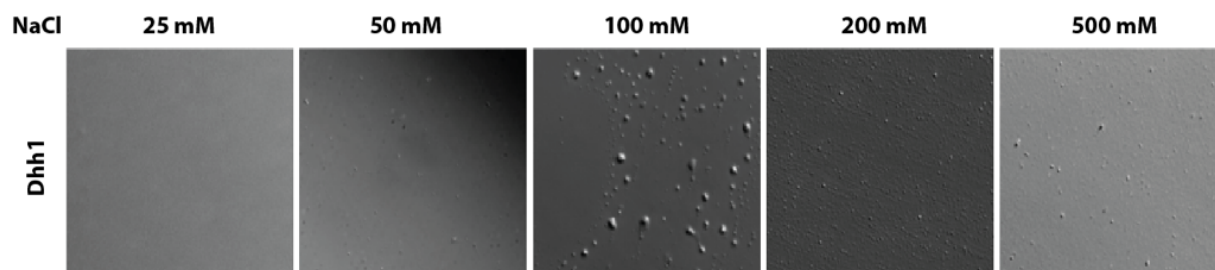


Fig.S 7.4. Dhh1 protein forms droplets under NaCl physiological conditions

Dhh1 protein, the stimulator of mRNA decapping, was purified using NI-NTA gravity column and ion exchange chromatography for further purification. The purified protein was subjected to different concentrations of NaCl, ranged from 25 mM to 500 mM. Dhh1 protein droplets were formed under physiological condition between 100 mM and 200 mM